Aspects of muon chemistry

Emil Roduner

University of Stuttgart, Germany

1 Muonium quantum effects

1.1 Introduction

Quantum effects are dynamic effects which occur whenever particles are confined in space. Any spatial constraint by potential walls of sufficient height gives rise to a discrete, mass dependent spectrum of energies. The simplest model of it is a particle constrained to remain in a one-dimensional square well. Depending on the shape of the confining potential, the functional dependence on the mass varies, but it is always true that the separation between energy levels is larger for the lower mass. If this separation is comparable to or larger than the thermal energy, then the equilibrium population of the particles over the energy levels has to be evaluated non-classically, and the behavior with temperature of various measurable quantities becomes mass dependent. A free particle, moving in an unbounded region of space, has a continuous spectrum of energy levels.

More relevant examples than particles in a square box are electrons confined in space by the nuclear Coulomb potential, nuclei which are bound in a molecule by a chemical bond, or atoms and ions which are trapped in a cage or in a crystal lattice.

The two most important quantum effects are related to zero-point energy and to tunnelling. They are most effectively revealed by isotope effects, that is by variations of properties such as hyperfine coupling constants, diffusion and chemical reaction rates when the mass of the particle changes, and they are particularly important for small masses. The muon mass is 1/9th the mass of a proton, or 1/18th the mass of a deuteron. Muonium, in a chemical sense, is a light isotope of atomic hydrogen and shows the same chemical behaviour, except when dynamics leads to isotope effects. The unprecedented mass ratio makes the muon and the Mu atom particularly sensitive probes of quantum phenomena. This is indeed an outstanding property, and experiments which take advantage of it are not easy to beat by other means.

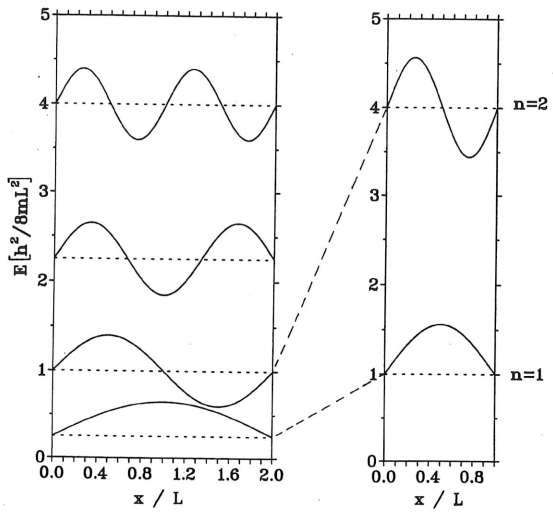

Figure 1. *Dependence of the energy levels of a particle in a one-dimensional box on the size of the box.*

1.2 Zero-point energy effects

Particles which are confined in a potential well have a zero-point energy which disappears in the classical limit of infinite mass, but it is very significant for muons and for Mu atoms confined in regions of space of atomic dimensions. For a particle of mass m in a one-dimensional square well of length L the eigenenergies are given by $E_n = n^2h^2/8mL^2$, where n is a non-zero integer quantum number. Figure 1 visualises the dramatic increase in kinetic energy when the spatial constraint increases.

For $L = 1$Å, the zero-point energy amounts to 21meV (2.0kJ/mol) for $m = m_p$, and to 186meV (17.9kJ/mol) for $m = m_\mu$. Nearly the same values are obtained for a one-dimensional harmonic oscillator with a force constant of 500N/m, representing the typical case of H or Mu atoms which are chemically bound to carbon.

The n-th energy of a hydrogen atom is given by $E_n = -\mu R_\infty/\mu_\infty n^2$, where R_∞ is the Rydberg constant, μ the electron-nuclear reduced mass (μ_∞ for infinite nuclear mass). From this we obtain the ionisation potential of an H atom to $I_p = -E_1 = 13.598$ eV, but the value for Mu is only 13.539eV, i.e. 59meV (5.7 kJ/mol) less.

If a potential well on a flat potential energy surface is not sufficiently deep it may happen that protons and deuterons can bind to it but the lowest allowed energy of the muon coincides with the rim so that there is no bound state.

While we are normally aware of the influence of zero-point energy on the ground state of a system we sometimes tend to forget that it affects also transition states. If the transition state is a bottle neck, for example when a diffusing atom has to squeeze through the lattice from one interstitial state to the next, the zero-point energy effect in the transition state can dominate, and diffusion of the light particle has a higher activation energy. The situation is depicted schematically in Figure 2.

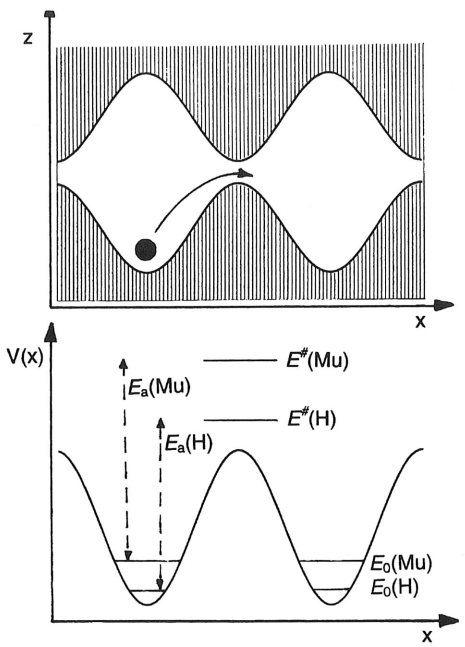

Figure 2. *Energetic consequence for a particle that passes through a bottle neck in the transition state.*

1.3 Tunnelling

A potential well that rises abruptly to infinity suppresses the wave function of a particle inside the wall to zero. However, infinite barriers do not occur in the real world, and thus the wave functions Ψ adopt a non-zero value inside the wall. According to the Born interpretation $\Psi^*(r)\Psi(r)$ represents the probability density of finding the particle at a position r in space. Thus, a non-zero value of Ψ inside the barrier of height V_0 represents a finite probability of finding the particle of energy $0 < E < V_0$ inside the barrier, with negative kinetic energy. This passage into a classically forbidden region is called *tunnelling*. If the barrier is not infinitely wide there exists a finite value for the particle to be found on the other side—it can tunnel through the barrier.

Tunnelling through a one-dimensional rectangular barrier of height V_0 and width L represents a model case which has been solved analytically. The transmission coefficient T gives the probability that a particle colliding with the barrier at kinetic energy E is found on the other side of the barrier. It is given by

$$T = \frac{4(1-x)}{4(1-x)+\sin^2 y} \quad \text{for } x > 1 \tag{1}$$

$$T = \frac{4(1-x)}{4(1-x)+\sinh^2 y} \quad \text{for } x < 1, \tag{2}$$

with the relative energy $x = E/V_0$ and $y = L\hbar^{-1}\sqrt{2mV_0|1-x|}$. The behaviour of T with

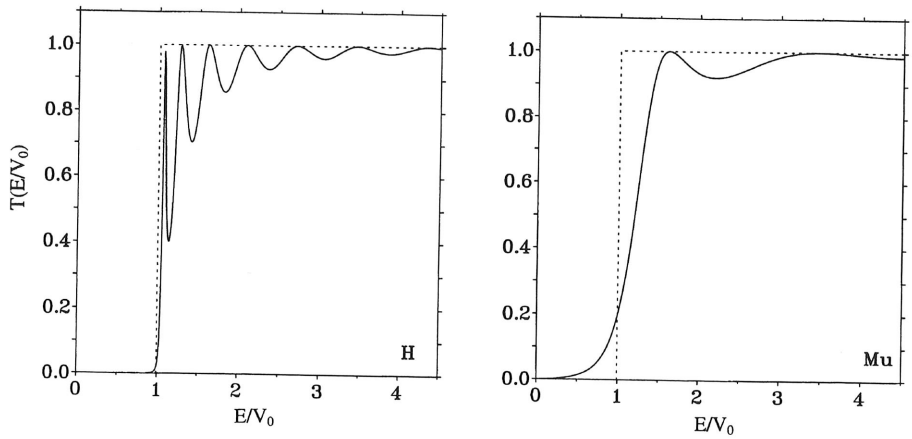

Figure 3. *Quantum mechanical transition probability as a function of energy for H 30(left) and Mu (right) through a rectangular one-dimensional barrier of 0.3eV height and 1Å thickness.*

energy is depicted for Mu and for H (or for μ^+ and p^+, respectively) in

Figure 3, based on a typical case of $V_0 = 0.3$ eV and $L = 1$Å. Transmission for $E < V_0$ ($x < 1$) is generally referred to as tunnelling since it is classically forbidden. The figure shows that it is much more significant for Mu than for H.

Classically, T equals unity for $E > V_0$. It is sometimes forgotten that quantum mechanically this is not the case. There are very pronounced oscillations with T significantly below unity at certain energies, in particular for the heavier particle. The resonance energies for $T = 1$ are given by $\sin y = 0$, i.e. by $y = n\pi$.

The main interest is in the isotope effect between H and Mu, which is plotted in Figure 4 as the ratio of transmission coefficients in logarithmic form as a function of energy. For the barrier chosen, Mu is favoured by seven orders of magnitude at low energies, but this selectivity decreases rapidly to unity as the energy approaches V_0. As a consequence of the oscillations in T, H is even favoured over Mu at energies just above the barrier. In reality, we often cope with isotope effects which result from measurements of systems in thermal equilibrium, where the particles have energies described by a Boltzmann distribution at a given temperature. This case is displayed by the broken line in Figure 4. It shows that the high transmission ratio for Mu at low energies dominates the effect even at temperatures which correspond to average energies $E > V_0$.

Further, the dependence of the transmission coefficient on the width of the barrier and on the mass of the tunnelling particle is of interest. The exact barrier width dependence is shown in Figure 5 (left) for Mu at three different energies and the mass dependence in Figure 5 (right) for a width of $L = 1$Å. For $x \leq 0.9$, the behaviour is given well by the approximate expression, $T = 16x(1-x)\exp(-2y)$. It is seen that the isotope effect is much larger, and the barrier width discriminates much better at low energies.

A more natural non-rectangular potential which gives a realistic picture of chemical reaction barriers was treated by Eckart (1940), and an analytical expression for the

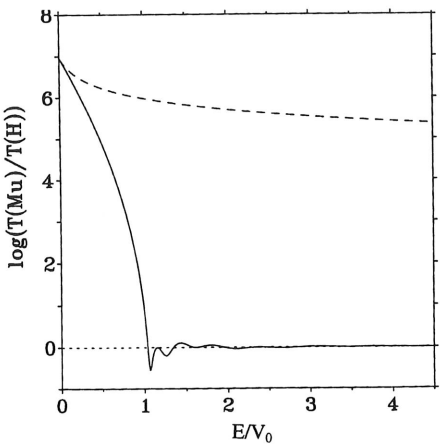

Figure 4. *Logarithmic plot of the Mu/H isotope effect for the transmission of a particle 26through a one-dimensional rectangular barrier of the same dimensions as in Figure 3. The solid line represents the effect for a discrete energy E, the broken line for a Boltzmann distribution with average energy E.*

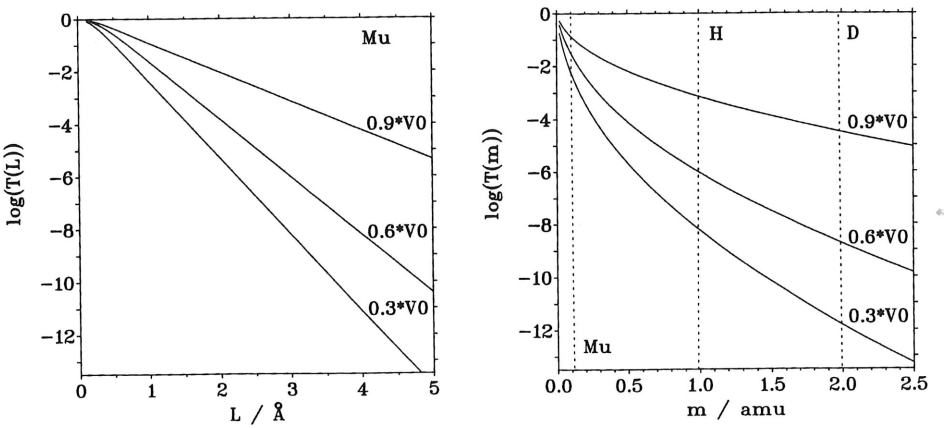

Figure 5. *Logarithmic plot for quantum mechanical transmission coefficients T for three different energies as a function of barrier thickness for Mu (left) and as a function of mass for L =1Å (right). The height of the barrier amounts to 0.3eV in all cases.*

transmission coefficient was derived.

We now focus briefly on **tunnel splitting in periodic potentials** which influence internal rotations of groups in molecules or translations of particles in crystalline solids. Figure 6 shows the example of a rotating methyl group in a threefold potential of 35meV (3.6kJ/mol). The lower energy states are well described by threefold degenerate wave functions which are localised in the three individual potential wells, and they may be approximated by the solutions for a harmonic oscillator with a force constant given by

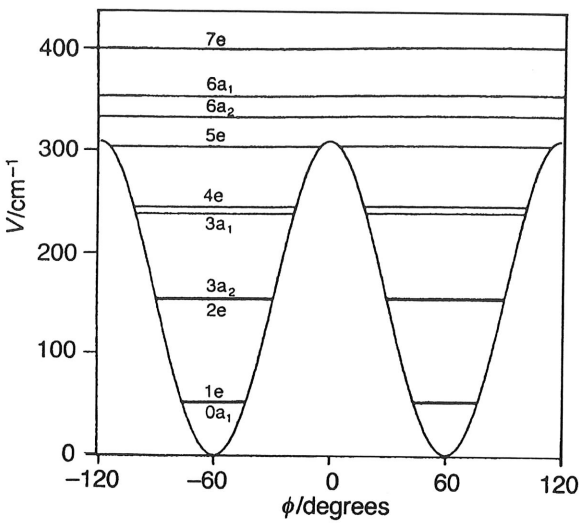

Figure 6. *Energy levels of a rotating methyl group in a threefold periodic potential. While the tunnel splitting is not resolved for the levels* $0a_1/1e$ *and* $2e/3a_2$ *it is clearly observed for* $3a_1/4e$ *and for the higher levels.*

the curvature of the potential at the minimum (i.e. the second derivative of a cosine function). At higher energies, where both the barrier width and $V_0 - E$ are lower, these individual wave functions overlap inside the barrier. This causes an interaction between the states, and the threefold degeneracy of the combined states of a and e symmetry is lifted by an amount which is called *tunnel splitting*. For energies much higher than V_0 the solution of the one-dimensional free rotator matches the situation.

For translational motion in a **periodic potential of a perfect crystal** the states are multiply degenerate. Tunnel splittings are no longer resolved since coupling of these numerous states leads to band-like structures.

1.4 Isotope effects on radical hyperfine couplings

Mu-substituted organic free radicals are perfect analogues of their H-substituted isotopomers. For a given structure of a radical, the muon-electron hyperfine coupling constants can be derived from the values tabulated for H by multiplication by the ratio of magnetic moments, $\mu_\mu/\mu_p = 3.1833$. On top of this trivial effect there is a so-called *intrinsic isotope effect* which increases the muon coupling by about another 20%. The origin is found in the anharmonicity of the potential energy curve representing the bond to the isotope. As shown in Figure 7 this leads to an asymmetry of the vibrational wave function and to an expectation value for the bond length which for the typical parameters of a C–H(Mu) bond is greater by approximately 5% (Roduner and Reid, 1989). When the bond is stretched further towards infinity one should in most cases expect a continuous increase of the muon hyperfine coupling until it reaches its limiting value for the Mu atom in vacuum.

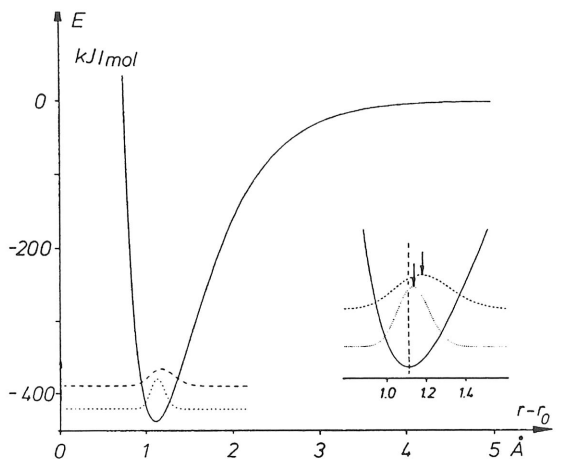

Figure 7. *Isotope effect on the bond length in a Morse potential with ground state vibrational wave functions ($|\Psi|^2$) for a diatomic C–H ($\cdots$) and C–Mu (- - -) fragment.*

Radicals where the Mu is atom bound in a group which rotates against the molecular frame exhibit an additional effect which is interpreted as a *conformational preference* in which the C–Mu bond more than a C–H or even a C–D bond has a trend to be eclipsed with the p_z-orbital containing the unpaired electron. Evidence is derived from the temperature dependence of the coupling constants, which was found to be opposite for a deuterium coupling in a DCH_2 rotor compared with that of the muon in a $MuCH_2$ rotor. An example is given in Figure 8 which displays the relevant reduced couplings of substituted *tert*-butyl radicals. The effect was shown to be related to zero-point energy (Claxton, 1987). The rotational dependence of the force constant of the C–H(Mu) stretching motion was shown to have a minimum when the bond is eclipsed with the p_z-orbital, and the molecule finds the lowest energy when the bond to the lightest particle adopts the eclipsed conformation.

1.5 Isotope effects on hyperfine couplings of encaged D/H/Mu

In general, the hyperfine coupling constants of atomic hydrogen in a host lattice deviate from their vacuum values, and the deviation is often isotope dependent. There is a number of reasons for these deviations. (i) Squeezing the atom in the lattice results in an increased spin density at the nucleus, and thus to a larger Fermi-contact interaction. (ii) Delocalisation of spin density onto neighbouring atoms allows for a decrease of the hyperfine interaction. (iii) Hydrogen atoms are quantum particles which vibrate even if squeezed in a lattice, and this leads necessarily to isotope dependent interactions with the environment. Such effects have been studied for atomic hydrogen in alkali halides, as shown in Figure 9, by Baumeler and by Spaeth (Baumeler *et al.* 1986, Spaeth, 1986). Similar investigations in liquid water (Figure 10) led to a determination of the size of the hydrophobic bubble containing the atom (Roduner *et al.* 1990).

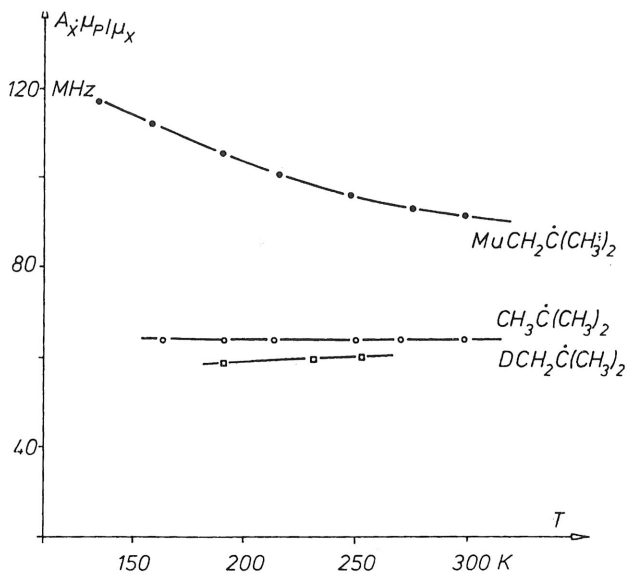

Figure 8. *Isotope effect on the reduced hyperfine coupling constant* $A'_\mu = A_\mu \times \mu_p/\mu_x$ *of a substituted rotating methyl group* XCH_2 *in a tertiary butyl radical.*

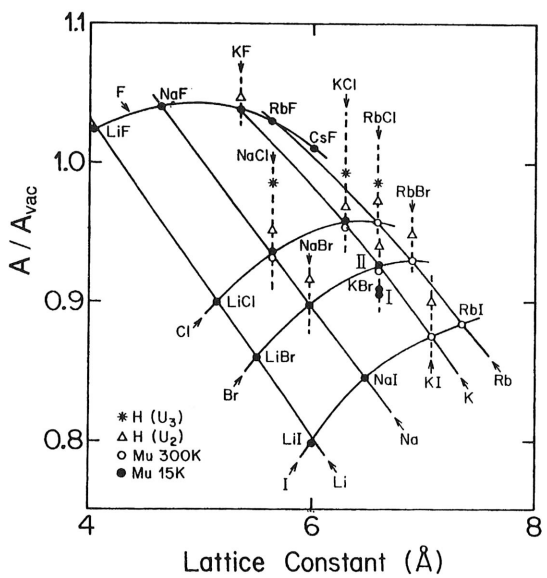

Figure 9. *Hyperfine parameters relative to their vacuum values for H and Mu centres in alkali halides (adapted from Baumeler et al. Hyperfine Interact. 32 (1986) 659).*

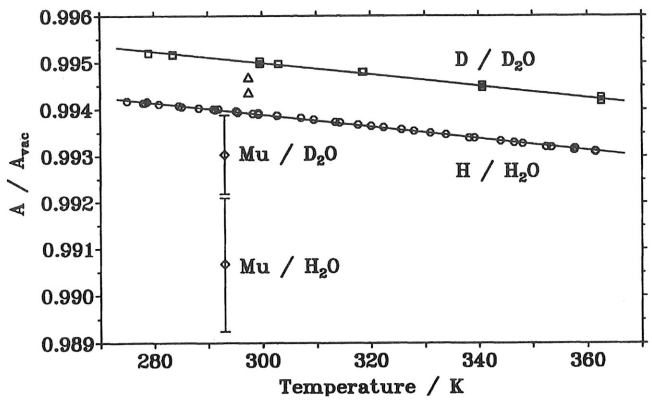

Figure 10. *Temperature dependence of hyperfine parameters relative to their vacuum values for hydrogen atoms in liquid water.*

1.6 Kinetic isotope effects

Primary isotope effects in which the chemical bond to the isotope is formed or broken are of particular importance in chemical reaction kinetics. Zero-point energy and tunnelling contribute both, mostly with the opposite effect. Thus, depending on the type of reaction, the lighter atom can be both faster or slower by up to two orders of magnitude, and more in special cases. A world record of a factor of 75000 (lower limit) at room temperature for a kinetic isotope effect is believed to be found for the transfer of H(Mu) bound in a cyclohexadienyl radical to dimethylbutadiene (Roduner and Münger, 1984).

In view of the above discussion of tunnelling through a one-dimensional rectangular barrier it is plausible that tunnelling dominates in addition reactions where the energy barriers are narrow, and not too high. This was unequivocally found to be the case in addition of hydrogen isotopes to benzene in the gas phase,

$$\mathrm{H} + \mathrm{C_6H_6} \longrightarrow \mathrm{C_6H_7} \tag{3}$$

$$\mathrm{Mu} + \mathrm{C_6H_6} \longrightarrow \mathrm{C_6H_6Mu} \tag{4}$$

as shown in the Arrhenius plot in Figure 11 (Roduner and Bartels, 1992). The signatures for tunnelling are the lower activation energy by nearly a factor of three for Mu as compared with H and D, and the lower frequency factor for the lighter atom (classically, as a result of the larger translational partition function, the lighter atom should have a higher frequency factor).

The potential barriers of hydrogen abstraction reactions are significantly higher and wider than those of addition reactions. An example is the abstraction from formate ions in aqueous solution (Lossack and Roduner):

$$\mathrm{D} + \mathrm{HCO_2^-} \longrightarrow \mathrm{DH} + \dot{\mathrm{C}}\mathrm{O_2^-} \tag{5}$$

$$\mathrm{H} + \mathrm{HCO_2^-} \longrightarrow \mathrm{H_2} + \dot{\mathrm{C}}\mathrm{O_2^-} \tag{6}$$

$$\mathrm{Mu} + \mathrm{HCO_2^-} \longrightarrow \mathrm{MuH} + \dot{\mathrm{C}}\mathrm{O_2^-}. \tag{7}$$

The Arrhenius plots given in Figure 12 show that the Mu reaction is much slower than those of the H and D isotopes, and its activation energy is higher. The isotope effect is

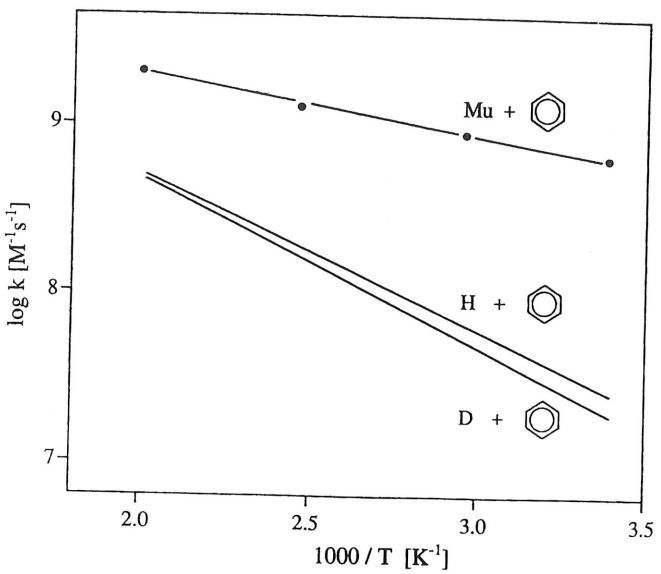

Figure 11. *Arrhenius plot of the rate constants for the addition of hydrogen isotopes to benzene in the gas phase (high pressure limit).*

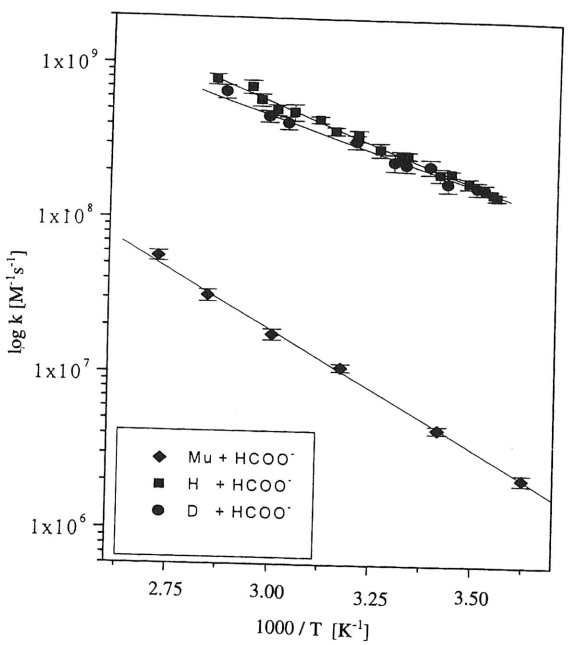

Figure 12. *Arrhenius plot for the rate constants of H abstraction from the formate ion in aqueous solution by the hydrogen isotopes Mu, H, and D.*

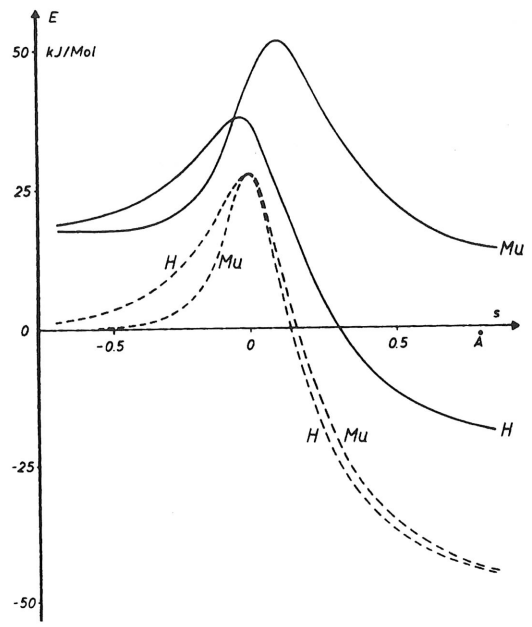

Figure 13. *Electronic barrier and vibrationally adiabatic barrier for the hydrogen abstraction from methanol by H and by Mu, given along the reaction coordinate s in a mass-weighted coordinate system.*

clearly dominated by zero-point energies in the transition state which are always higher for the lighter isotope.

It should be noted that the moving mass changes along the reaction coordinate. For the example of Figure 12 Mu moves relative to HCO_2^- in the entrance channel of the reaction, but in the exit channel it is MuH which moves relative to CO_2^-. Thus, for estimations of tunnel coefficients, one has to work in a properly scaled (mass weighted, see Glasstone et al. 1941) coordinate system in which the reduced mass is constant along the reaction coordinate. Its effect is seen in Figure 13, which shows that the electronic barrier (broken lines) is narrower for Mu (reduced mass of 1.02a.m.u., evaluated for H abstraction from methanol) than for H (reduced mass of 1.71a.m.u.). Furthermore, what counts is the *vibrationally adiabatic* barrier. It is the sum of the electronic potential energy and the zero-point energies of all vibrational degrees of freedom except the reaction coordinate. This is given by the solid line in Figure 13.

1.7 Dynamic solvent effects

Mu, in contrast to H, is suitable to probe dynamic solvent effects in aqueous solution. The concept of *solvent friction* is known since 1940 and was introduced by Kramers (1940). In principle, it is a classical effect, but it affects Mu to a much larger extent than H. This was probed by measuring the addition kinetics of H and Mu to benzene (Roduner and Bartels, 1992). It was found for H that the reaction is faster by a factor of approximately 35 in

aqueous solution compared with the gas phase, and this was explained by an equilibrium solvent effect (H does not solvate well and tends to get expelled from water). Much of this is a solvent entropy effect, involving the reorientation of water molecules under formation of a hydrophobic solvent cage. Based on this one would expect the same acceleration factor for Mu, but it was found to be less than a factor of five. This originates in the faster motion across the reaction barrier of the light Mu atom—the reorientation/relaxation of the water molecules is not able to follow, so the Mu reaction cannot take full advantage of the negative solvation entropy. This non-equilibrium effect was confirmed in recent theoretical work by Garrett and Schenter (1994).

1.8 Diffusion in liquids

Isotope effects are expected and observed routinely for diffusing species in the gas phase and in solids. There is no principal reason why they should not occur in liquids, but in fact the mass-independent Stokes-Einstein formula, often with a small mass-independent correction factor for friction, works so well that it is mostly used for liquids. It proved to be hard to find unambiguous evidence for a mass-dependence. Analysis of the diffusion controlled reaction of Mu with oxygen in water, and comparison with the corresponding reaction for H, provided this evidence and showed that the lighter hydrogen isotope diffuses faster in liquids (Roduner et al. 1995a).

2 Avoided level crossing spectroscopy

2.1 The origin of avoided level crossing (ALC) effects

It is often useful to write the exact Hamiltonian of a quantum mechanical system as

$$\widehat{H} = \widehat{H}^0 + \widehat{H}^1. \tag{8}$$

With $\widehat{H}^1 \ll \widehat{H}^0$, this is the basis for perturbation theoretical treatments, and the time independent Schrödinger equation $\widehat{H}^0\chi_n = E_n^0\chi_n$ defines a set of zero-order eigenfunctions χ_n to $\widehat{H}^0$ which are good approximations to the eigenfunctions Ψ_n to $\widehat{H}$ and represent the system very well over a large range of experimental parameters. The effect of $\widehat{H}^1$ leads to corrections to the zero order energies which are given up to second order by

$$E_n - E_n^0 = \langle\chi_n|\widehat{H}^1|\chi_n\rangle + \sum_m \frac{|\langle\chi_n|\widehat{H}^1|\chi_m\rangle|^2}{E_n^0 - E_m^0}. \tag{9}$$

This correction is normally very small, but for a crossing of zero-order energy levels, i.e. for $E_n^0 = E_m^0$, the expression diverges if the matrix element in the numerator is not zero. Even though the above treatment breaks down it can easily be imagined that, near this crossing, the corrections are considerable, and dramatic effects may be expected to occur in certain experiments.

It turns out that the energy levels E of the exact solution Ψ to $\widehat{H}$ do not cross but repel each other. We say that $\widehat{H}^1$ leads to an *avoided level crossing* (others call it *level crossing* or *anticrossing*). The effect is displayed schematically in Figure 14.

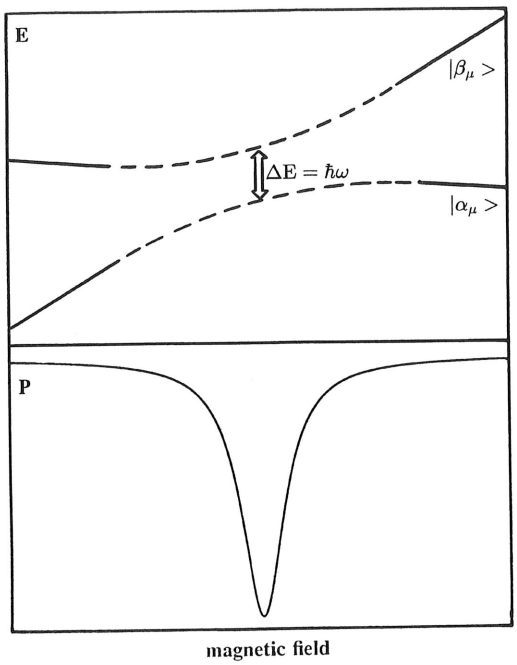

Figure 14. *Schematic representation of an avoided level crossing and its effect on the muon spin polarisation in a time-integrated longitudinal field μSR experiment.*

Most often, the experimental parameter that allows the tuning through an avoided crossing is a magnetic field, in some cases an electric field. Severe consequences relate to the break-down of the Born-Oppenheimer approximation which arises in avoided crossings of electronic energy surfaces as a function of internuclear distances.

Probably the first observation and treatment of an avoided level crossing effect is attributed to Eck et al. (1963) in optical resonance fluorescence. The merit for introduction of the effect to μSR belongs to Abragam (1984).

In high field magnetic resonance, the spin eigenstates Ψ_n are to a good approximation pure Zeeman states χ_n, and their energies vary linearly with field. This leads to true crossings of states. ALC–μSR experiments usually work with longitudinally polarised muons. Muons with their spins parallel or antiparallel to the field are in eigenstates, and there is no time dependence of the wave function.

Avoided crossings are represented by field-dependent mixtures of two Zeeman states. Let us assume that the muons are all initially in spin state α, which now represents a non-eigenstate of the system. This leads to oscillations of the system between the two eigenstates α and β and thus of the muon spin direction. Three conditions must be obeyed for effects to be observed in longitudinal-field μSR experiments: (i) there must be an element in the Hamiltonian which leads to a mixing of states, (ii) this element must be sufficiently large to cause a minimum separation ΔE of the levels so that the oscillation between the states occurs with a frequency ν_r, or in a time $\nu_r^{-1} = h/\Delta E$ which is short or comparable to the muon lifetime, and (iii) one of the eigenstates must belong to muon

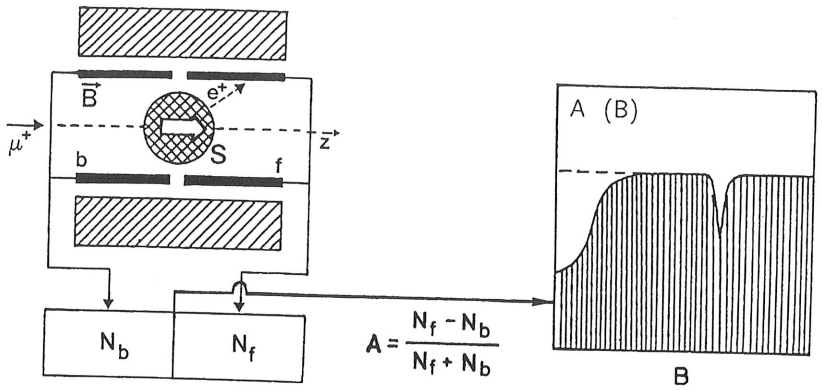

Figure 15. *Experimental setup for time-integrated ALC–μSR experiments. The muons are stopped in the sample S which is placed in a magnetic field parallel to the muon spin direction. Decay positrons are counted in two sets of counters in the forward (f) and backward (b) direction of the sample with respect to the incoming beam. The muon decay asymmetry A, the difference over the sum of the two count rates, is plotted as a function of the external field B as shown in the right-hand part of the figure.*

spin α, the other one to β, other avoided crossings are μSR-inactive.

We distinguish between two types of avoided crossings, one in which there is an off-diagonal element in the energy matrix as written in the conventional Zeeman basis which mixes the two states directly, and a second one where the mixing occurs indirectly via coupling of both states to a common, energetically remote state.

ALC effects may be observed either directly in a time-resolved mode, or more conventionally in a time-integrated mode, counting only the forward-backward muon decay asymmetry while the external magnetic field is swept. The avoided crossings lead to relaxation dips, or resonances, in a plot of the decay asymmetry (or the normalised muon polarisation) as a function of field. A schematic experimental setup and the general shape of a ALC–μSR spectrum are given in Figure 15.

2.2 The use of ALC spectroscopy

Transverse field muon spin rotation observes a muon nuclear magnetic resonance transition, which in multi-spin paramagnetic systems is equivalent to a electron-nuclear double resonance (ENDOR) transition. In high fields, the only information that is obtained about the Hamiltonian is the muon-electron hyperfine interaction. In principle, the hyperfine parameters of other magnetic nuclei are obtained in low or zero field, but in most cases the muon polarisation is distributed over far too many frequencies so that the individual precession signals have insufficient amplitude for observation. Moreover, the paramagnetic species normally have muonium as a precursor. In this case, in order to ensure coherent transfer of muon polarisation, the product species has to be formed fast on the time scale of muon precession in Mu; usually this means in less than one nanosecond.

ALC–μSR gives the magnetic interactions of all the other magnetic nuclei which are

coupled to the unpaired electron, as long as the coupling constants are not too small. Quadrupolar interactions are obtained as well. The technique thus yields detailed structural information about organic free radicals, or about muon-centred paramagnetic defects in semiconductors and insulators.

The dephasing problem of transverse field μSR does not apply to longitudinal fields. It is sufficient for the observation of a species that it is formed on a time scale fast or comparable to the time evolution of polarisation in the radical. Usually, formation within one microsecond of the muon stop event is sufficient. ALC–μSR is thus a suitable technique for *final state spectroscopy*, that is for the detection of states which are depolarised and thus not observable in transverse fields due to too slow formation.

In most cases the strongest resonance observed in solid samples is absent in isotropic (liquid or gaseous) environments. If there is reorientation dynamics on a time scale of the order of the inverse hyperfine anisotropy, typically 20-50 nanoseconds, then this resonance is an extremely sensitive indicator of reorientation dynamics and of residual anisotropy.

2.3 Resonance fields and selection rules

ALC resonances can be observed for diamagnetic systems with quadrupolar coupling terms, but mostly they have been studied for paramagnetic systems in solids, liquids, and gases. Let us therefore start with the Hamiltonian of a spin system consisting of a muon with spin I^μ and isotropic hyperfine coupling A_μ, an electron with spin S, and n nuclei with spin I^k and isotropic hyperfine coupling A_k, and for simplicity we shall assume axial symmetry with perpendicular dipolar components $D^i_\perp$ $(i = \mu, k)$:

$$\begin{aligned}
\widehat{H}/h &= \nu^e \widehat{S}_z - \nu^\mu \widehat{I}^\mu_z - \textstyle\sum_k \nu^k \widehat{I}^k_z + A_\mu \widehat{S}_z \widehat{I}^\mu_z + \textstyle\sum_k A_k \widehat{S}_z \widehat{I}^k_z \\
&\quad + \tfrac{1}{2} A_\mu [\widehat{S}_+ \widehat{I}^\mu_- + \widehat{S}_- \widehat{I}^\mu_+] + \tfrac{1}{2} \textstyle\sum_k A_k [\widehat{S}_+ \widehat{I}^k_- + \widehat{S}_- \widehat{I}^k_+] \\
&\quad - D^\mu_\perp [A^\mu + B^\mu + C^\mu + D^\mu + E^\mu + F^\mu] \\
&\quad - \textstyle\sum_k D^k_\perp [A^k + B^k + C^k + D^k + E^k + F^k] \\
A^i &= (1 - 3\cos^2\theta) \widehat{S}_z \widehat{I}^i_z \\
B^i &= -\tfrac{1}{4}(1 - 3\cos^2\theta)[\widehat{S}_+ \widehat{I}^i_- + \widehat{S}_- \widehat{I}^i_+] && \Delta M = 0 \\
C^i &= -\tfrac{3}{2}(\sin\theta\cos\theta e^{-i\phi})[\widehat{S}_z \widehat{I}^i_+ + \widehat{S}_+ \widehat{I}^i_z] && \Delta M = 1 \\
D^i &= -\tfrac{3}{2}(\sin\theta\cos\theta e^{+i\phi})[\widehat{S}_z \widehat{I}^i_- + \widehat{S}_- \widehat{I}^i_z] && \Delta M = 1 \\
E^i &= -\tfrac{3}{4}(\sin^2\theta e^{-2i\phi})[\widehat{S}_+ \widehat{I}^i_+] && \Delta M = 2 \\
F^i &= -\tfrac{3}{4}(\sin^2\theta e^{+2i\phi})[\widehat{S}_- \widehat{I}^i_-] && \Delta M = 2
\end{aligned} \tag{10}$$

where θ is the angle between the symmetry axis and the field, ϕ the azimuthal angle.

First we solve the problem for the *isotropic* case ($D^i_\perp = 0$), and for a single type of non-muon nucleus (or equivalent nuclei) with spin I^k and corresponding z-component m^k. We write the secular determinant in a Zeeman product basis $|\chi^e_i\rangle|\chi^\mu_i\rangle|\chi^k_i\rangle$. The off-diagonal elements mix the basis functions with equal $M = m^s + m^\mu + m^k$. Therefore the determinant factorises into $2M + 1 = 2I^k + 3$ subdeterminants. Two of them are of rank 1 ($|M| = I^k + 1$), two of rank 3 ($|M| = I^k$), and $2I^k - 1$ of rank 4 ($|M| < I^k$). An example of the latter is given in Table 1 before and after block diagonalisation. The form of the operators in the off-diagonal elements, $\widehat{S}_+ \widehat{I}^i_-$ and $\widehat{S}_- \widehat{I}^i_+$, determines the selection rule, $\Delta M = \Delta(m^\mu + m^k) = 0$, in short Δ_0, for this muon-nuclear spin flip-flop transition in which the spin polarisation oscillates between the muon and the magnetic nucleus in resonance, mediated by the unpaired electron. The crossing of the energy levels is lifted

by the product of the *isotropic* muon and nuclear hyperfine coupling constants, and the levels mix via coupling of the two states to a common remote state with opposite electron spin (Note that the direct off-diagonal elements between the states χ_1 and χ_2 are zero). These resonances are therefore observable not only in the anisotropic solid state but also in the liquid or gaseous phases.

(a)

	$\lvert\frac{1}{2},-\frac{1}{2},M\rangle$ χ_1	$\lvert\frac{1}{2},\frac{1}{2},M-1\rangle$ χ_2	$\lvert-\frac{1}{2},\frac{1}{2},M\rangle$ χ_3	$\lvert-\frac{1}{2},-\frac{1}{2},M+1\rangle$ χ_4
χ_1	$E_{11}-E$	0	$A_\mu/2$	$bA_k/2$
χ_2	0	$E_{22}-E$	$cA_k/2$	0
χ_3	$A_\mu/2$	$cA_k/2$	$E_{33}-E$	0
χ_4	$bA_k/2$	0	0	$E_{44}-E$

where

$$\begin{aligned} M &= m^s + m^\mu + m^k \\ E_{ii} &= m^s\nu^e - m^\mu\nu^\mu - m^k\nu^k + m^s m^\mu A_\mu + m^s m^k A_k \\ b &= \left[I^k\left(I^k+1\right) - M(M+1)\right]^{1/2} \\ c &= \left[I^k\left(I^k+1\right) - M(M-1)\right]^{1/2} \end{aligned}$$

(b)

	Ψ_1	Ψ_2
Ψ_1	$E_{11} + A_\mu^2/4\nu^e + b^2A_k^2/4\nu^e - E$	$cA_\mu A_k/4\nu^e$
Ψ_2	$cA_\mu A_k/4\nu^e$	$E_{22} + c^2A_k^2/4\nu^e - E$

Table 1. *Elements of the secular determinant in the basis* $|m^s, m^\mu, m^k\rangle$ *before (a) and after (b) block-diagonalisation.*

The resonance field for this case was obtained in the detailed initial treatment by Heming et al. (1986):

$$B_r(\Delta_0) = \left|\frac{A_\mu - A_k}{2(\gamma_\mu - \gamma_k)} - \frac{A_\mu^2 - 2MA_k^2}{2\gamma_e(A_\mu - A_k)}\right|, \tag{11}$$

where $\gamma_\mu = 13.55$kHz/G, $\gamma_k = 4.26$kHz/G for protons, and $\gamma_e = 2802.49$kHz/G, are the gyromagnetic ratios for the three types of spins.

Due to the dependence on M there are $2I^k$ nearly degenerate resonances. The corresponding minimum energy gap of the avoided crossing and thus the ALC oscillation frequency on resonance is to a good approximation given by

$$\nu_r(B_r, \Delta_0) = \frac{cA_\mu A_k}{2B_r\gamma_e}. \tag{12}$$

If one of the two coupling constants is low this will result in a low value of ν_r and thus often in a low amplitude of the resonance.

We now focus on a different type of transition which is only possible under conditions of hyperfine anisotropy. No magnetic nucleus other than the muon participates in it. We

therefore drop all terms relating to nuclei k in the Hamiltonian (Equation 3). The terms C^μ and D^μ lead to new off-diagonal elements which were not present in the isotropic case. The effective operators are I^μ_+ and I^μ_-. The transition can thus be called a muon spin flip, and the corresponding selection rule is $|\Delta M| = 1$, or Δ_1. The resonance field is easily obtained by diagonalisation of the two subdeterminants of rank two. It is in both cases

$$B_r(\Delta_1) = \left[A_\mu + D_\perp(3\cos^2\theta - 1)\right]\left[\frac{1}{2\gamma_\mu} - \frac{1}{2\gamma_e}\right], \tag{13}$$

and the corresponding gap frequency on resonance is

$$\nu_r(B_r, \Delta_1) = \frac{3}{2} D_\perp \sin\theta\cos\theta. \tag{14}$$

Both expressions are orientation dependent, and we see immediately that the resonance disappears for $D_\perp = 0$ and for $\theta = n\pi/2$.

In presence of nuclei k with anisotropic couplings there are also muon-nuclear spin flip-flip resonances with selection rule $|\Delta M| = 2$ arising from the terms $E^{\mu,k}$ and $F^{\mu,k}$ in the Hamiltonian. It turns out that they are very narrow and weak and thus rarely observed in experiments. To within a few percent, the resonance positions can be analysed based on the following approximate expression, neglecting the correction terms which are proportional to γ_e^{-1}:

$$B_r(\Delta M) = \frac{1}{2}\left|\frac{A_\mu + (|\Delta M| - 1)A_k}{\gamma_\mu + (|\Delta M| - 1)\gamma_k}\right|, \tag{15}$$

which holds also for the Δ_2 lines. This reduces to $B_r(\Delta_0) = (A_\mu - A_k) \times 53.80$ Gauss/MHz for muon-proton transitions, to $B_r(\Delta_1) = A_\mu \times 36.72$ Gauss/MHz for muon spin flips, and to $B_r(\Delta_2) = (A_\mu + A_k) \times 28.08$ Gauss/MHz for muon-proton spin flip-flip resonances.

The three types of high field avoided crossings for an electron-muon-proton system are shown in the upper part of Figure 16. Only the levels with electron spin α are shown. Since the electron Zeeman term dominates the levels with electron spin β are well separated and do not cross those with electron spin α.

For paramagnetic species in low fields the eigenstates are generally mixtures of Zeeman basis states, the muons therefore oscillate and the observed decay asymmetry is reduced (see schematic signal in Figure 15).

2.4 ALC–μSR line shapes

The time dependent longitudinal muon polarisation expressed in a basis of Zeeman product states $\Psi_n = \sum_i c_{in}\chi_i$ is evaluated using a density matrix method. It yields

$$\begin{aligned} P_z(B,t) \;=\; & \frac{1}{N}\sum_n \left|\sum_i 2c^*_{in}c_{in}m^\mu_i\right|^2 \\ & + \frac{2}{N}\sum_{m<n}\left|\sum_i 2c^*_{in}c_{im}m^\mu_i\right|^2 \cos(\omega_{nm}t - \phi_{nm})e^{-\lambda_{nm}t}, \end{aligned} \tag{16}$$

where N is a normalisation factor of the wave function, λ_{nm} is the relaxation rate of the oscillating signal, and ϕ_{nm} its initial phase which depends on the geometry of the

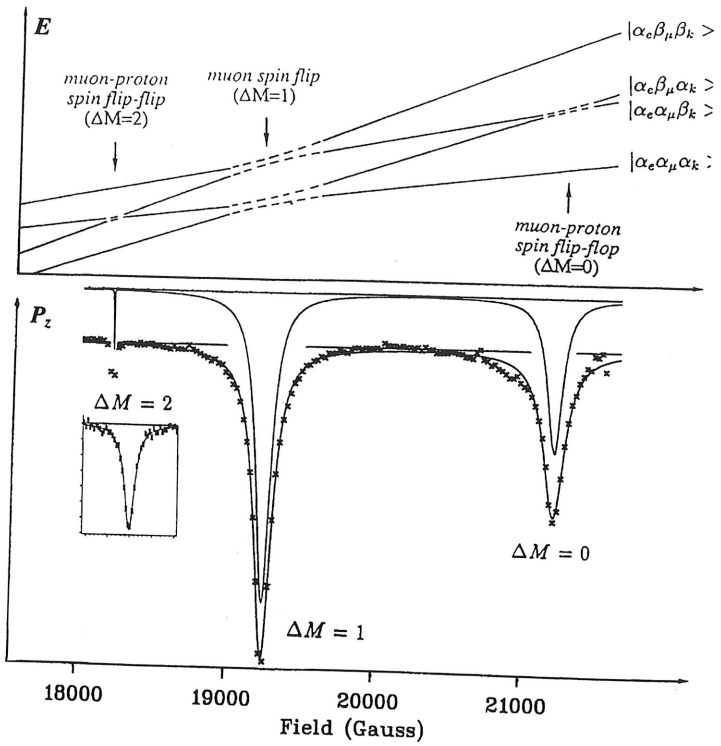

Figure 16. *Avoided crossings of the energy levels of an electron-muon-proton three spin-$\frac{1}{2}$ system with the selection rules indicated (upper part), and corresponding experimental and simulated ALC resonances for single crystal benzene as reported by Roduner (1990). The inset shows the experimental $|\Delta M| = 2$ resonance.*

experimental arrangement. Outside avoided crossings the coefficients c_{in} are either zero or one so that the time dependent term disappears, and $P_z(B)$ becomes unity.

The time histogram of a μSR experiment is given by

$$S_{f,b}(t) = N_0 \exp(-t/\tau_\mu)[1 \pm aP_z(B,t)], \tag{17}$$

where τ_μ is the muon lifetime and a an experimental asymmetry factor. The ALC–μSR signal is obtained from the forward-backward muon decay asymmetry

$$A = \frac{N_b - N_f}{N_b + N_f}, \tag{18}$$

with the number of positron counts $N_{f,b}$ in the two telescopes given by the time integral over the histograms

$$N_{f,b} = \frac{\int_0^\infty S_{f,b}(t)dt}{\int_0^\infty \exp(-t/\tau_\mu)dt}. \tag{19}$$

Using the theoretical expression for $P_z(B,t)$, integration over the oscillating and relaxing signal gives

$$\bar{P}_z(B) = 1 - \frac{\frac{2}{N}\sum_{i=1}^{2I^k} \nu_r^2}{(\lambda_{nm}/2\pi)^2 + \nu_r^2 + \{(B - B_r)[(\gamma_\mu + (|\Delta M| - 1)\gamma_k)]\}^2}. \quad (20)$$

This represents a Lorentzian shape of the resonance which holds for single crystals, and for Δ_0 transitions in the liquid and gaseous phases. A typical example showing all three types of resonances was obtained with single crystal benzene and is given in the lower part of Figure 16. For powders, the signal has to be integrated over all orientations. This leads to often characteristic non-Lorentzian line shapes.

2.5 Studies of dynamic systems

2.5.1 Relaxation

Relaxation processes play an important role in spin systems, in fact, magnetic resonance experiments are virtually impossible in the absence of any relaxation. Stochastic fluctuations lead to a dissipative coupling of a spin system to a *heat bath* or a *lattice* and to spin relaxation in longitudinal fields. These processes are therefore called *spin-lattice relaxation*, and the corresponding relaxation times are referred to as T_1.

Relaxation theories are well developed for a large variety of processes and systems. However, the treatments normally relate to high field conditions where pure Zeeman product states are satisfactory representations of a system. The vast majority of experiments are indeed conducted under high field conditions. Unfortunately, this is not true for ALC–μSR experiments. Even though they are conducted in high fields the eigenfunctions are mixtures of two Zeeman states, and the mixing coefficients vary between 0 and 1 as the system is tuned through the avoided crossing. As a consequence of this, relaxation theories in their conventional form are useless, and the theories have to be rewritten to account for this more complex case.

Colloquially, it is often said that ALC–μSR resonances arise from muon spin *relaxation*. More precisely, we should keep in mind that they occur also for isolated spin systems in the absence of stochastic perturbations in a heat bath. The time evolution of spin polarisation is then periodic and undamped, and the time-integral polarisation itself oscillates. It is only by virtue of the muon decay that defined resonances are observed. The muon life sets a critical time scale for time evolution and gives a higher weight to fast oscillations whereas slow processes may appear static even if integration formally goes to infinite time.

Δ_0 resonances relate to oscillations of the spin polarisation between the muon and the magnetic nucleus (or a set of equivalent nuclei). Since they arise under isotropic conditions there is no transverse component of the polarisation as long as the muons are implanted with their spins parallel to the external field. For Δ_1 resonances this is different: due to anisotropy, the hyperfine field is at an orientation-dependent angle to the external field, and the periodic evolution represents a precession about the *effective* field resulting from vector addition of hyperfine and external field (Kreitzman and Roduner, 1995).

Stochastic fluctuations perturb and interrupt the periodic time evolution, which leads to a damping and thus to a change in shape of the ALC resonances. The relaxation processes are no different from those of relevance in more conventional variants of magnetic resonance, encompassing for example intermolecular and intramolecular dipolar interaction, quadrupolar interactions, spin-rotation or spin-exchange mechanisms, and stochastic

modulation of the isotropic couplings.

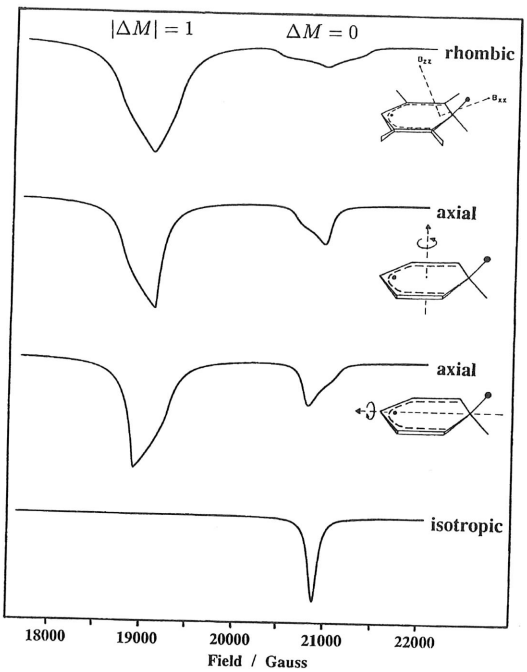

Figure 17. *Simulated part of the spectrum expected for benzene in the field range of the two major resonances. The entries relate to the static case (first entry, rhombic), the axial cases for rotation about two different axis (second and third entries), and to the isotropic case as expected for the liquid and the gaseous phases.*

2.5.2 Reorientation dynamics

The dipolar part of the hyperfine interaction describes the distribution of the unpaired electron spin density as seen from the magnetic nucleus. It therefore provides a tensor which has a fixed and usually well-known orientation with respect to the static radical, and which is traceless. Rapid rotation of the molecule about a certain axis leads to partial averaging of this tensor, and in any case to axial symmetry. The critical time scale for this process is related to the inverse of the level splitting at the avoided crossing. For a Δ_1 transition the corresponding correlation time is $\tau_c = (2\pi D_\perp)^{-1}$, which is often of the order of 20-50ns. For a Δ_0 resonance τ_c may be of the order of one microsecond. The component of the dipolar hyperfine ellipsoid which is parallel to the rotation axis is invariant towards rotation and determines $D_\parallel = -2D_\perp$.

Figure 17 displays simulations for the Δ_1 and the most prominent Δ_0 transition. It shows the resonances for the static case and for fast rotation about two different axes. It demonstrates that the preferred rotational axis is immediately obtained from the line shape.

Any wobbling, tumbling or reorientational jump motion of the parallel axis leads to a more extensive averaging of the hyperfine tensor and thus to a further reduction of $D_{\parallel}$. As long as this motion is fast compared with the critical time scale the Δ_1 line shape remains axial, but it has a reduced width which corresponds to a new effective hyperfine anisotropy. The effective anisotropy will decrease with increasing amplitude of the averaging motion. The situation may be called *pseudo-static* since it is not possible to extract any correlation time from the spectrum.

A reorientational motion that has a correlation time which is comparable with the critical time scale of the experiment will often have a dramatic effect on the ALC spectrum. The resonances may become very strong and broad, and the (muon) nuclear T_1 relaxation times may be considerable over a very large field range. Dynamic effects have been treated semi-analytically for isotropic reorientational motion (Kreitzman and Roduner, 1995) and using Monte Carlo techniques for more complex dynamic models (Tregenna-Piggott *et al.* 1995). Such an analysis permits the determination of correlation times as a function of temperature.

Simulations of a Δ_1 resonance for the two limiting cases are displayed in Figure 18. In the pseudo-static case the resonance narrows with increasing amplitude of the averaging motion, and it disappears as a small, narrow vee (upper graph). Isotropic rotational diffusion leads to the disappearance of the resonance with decreasing correlation times via broadening.

As demonstrated in Figure 4, fast isotropic reorientational motion leads to the disappearance of the Δ_1 transition, while the Δ_0 resonances remain allowed and adopt a Lorentzian line shape.

2.5.3 Chemical kinetics and Heisenberg spin exchange

Chemical reactions limit the lifetime of a species, which must lead to broadening also of ALC–μSR lines. The same holds for the lifetime of spin states in spin exchange collisions. Since the latter is field dependent but the former is not, the two processes can be distinguished in field dependent experiments. This was demonstrated for the interaction between molecular oxygen and ethyl radicals in the gas phase (Dilger *et al.* 1996). The actual kinetic parameters, however, were obtained more reliably by direct T_1 relaxation measurements off-resonance than by time integrated ALC experiments.

A site-jump of a muon species or an organic radical that switches conformation leads to sudden changes in the coupling constants and thus to a jump between ALC resonances. At low jump rates this leads to broadening of the signals, but at higher rates an averaged signal may appear and show motional narrowing effects. Such a situation was simulated by Roduner (1990) but to our knowledge has not been encountered in experiments so far.

2.6 Examples

Figure 19 displays a spectrum obtained with 6,6-dimethylfulvene in diethylether solution. Two radicals were observed by transverse field μSR, but four inequivalent unsaturated carbon atoms are available for Mu addition to the molecule. By analysis of the ALC spectrum and based on literature values for similar radicals it was possible to show that

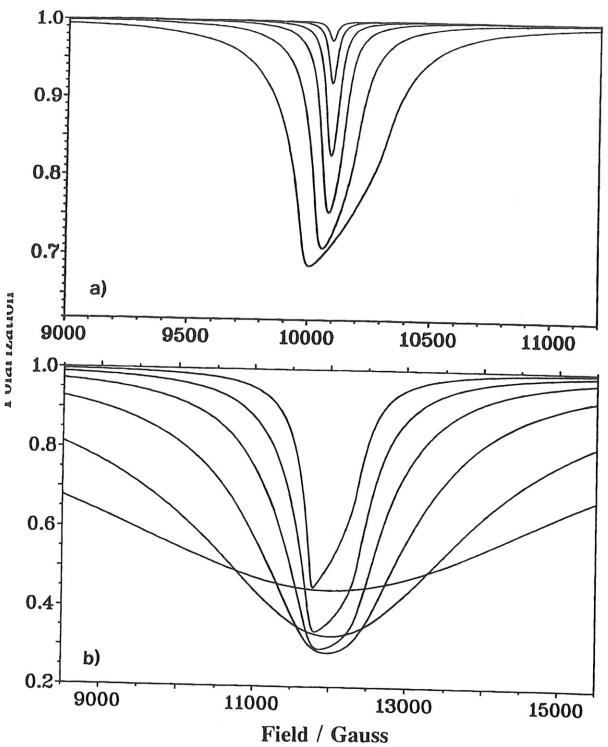

Figure 18. *(a) Simulations of pseudo-static powder patterns for the Δ_1 ALC–μSR resonance of a muon-electron system with $A_\mu = 275MHz$ and axial hyperfine anisotropies $D^\mu_\perp$ of -3.0, -1.5, -0.4, -0.2, and -0.1MHz, going from the broad outer to the narrow inner curves. (b) Simulation, using a stochastic Liouville mechanism, of an axial Δ_1 powder line shape for spherical rotational diffusion, based on $A_\mu = 326MHz$ and $D^\mu_\perp$ of -5.4MHz. The rotational diffusion constants $D_{rot} = 1/6\tau_c$ are 0.0, 0.3, 1.0, 3.0, 10, and 30MHz, going from the inner to the outer curves (adapted from Roduner et al. 1995).*

addition occurs exclusively at the ring carbons (Roduner, 1993). The two gaps in the spectrum are indicative of small proton couplings which lead to low amplitude resonances (compare Equation 5).

Two kinds of Mu with slightly different muon hyperfine couplings which are below the vacuum value by more than a factor of three were observed in CuCl. By means of ALC–μSR it was possible to show that both species are located at tetrahedral interstitial sites with four Cu nearest neighbours and six Cl next-nearest neighbours (Schneider *et al.* 1990). Figure 20 demonstrates the richness of information that is available from single crystal experiments of this material.

An illustrative example of the two kinds of dynamics as introduced in Section 5.2 and Figure 18 was obtained with the Mu adduct radicals to the fullerenes C_{60} and C_{70} (addition to carbons next to the equator) in the polycrystalline state under conditions where there is fast rotation (Figure 21). The C_{60} adduct shows line broadening with increasing temperature, as expected for isotropic rotational diffusion, while the C_{70} adduct

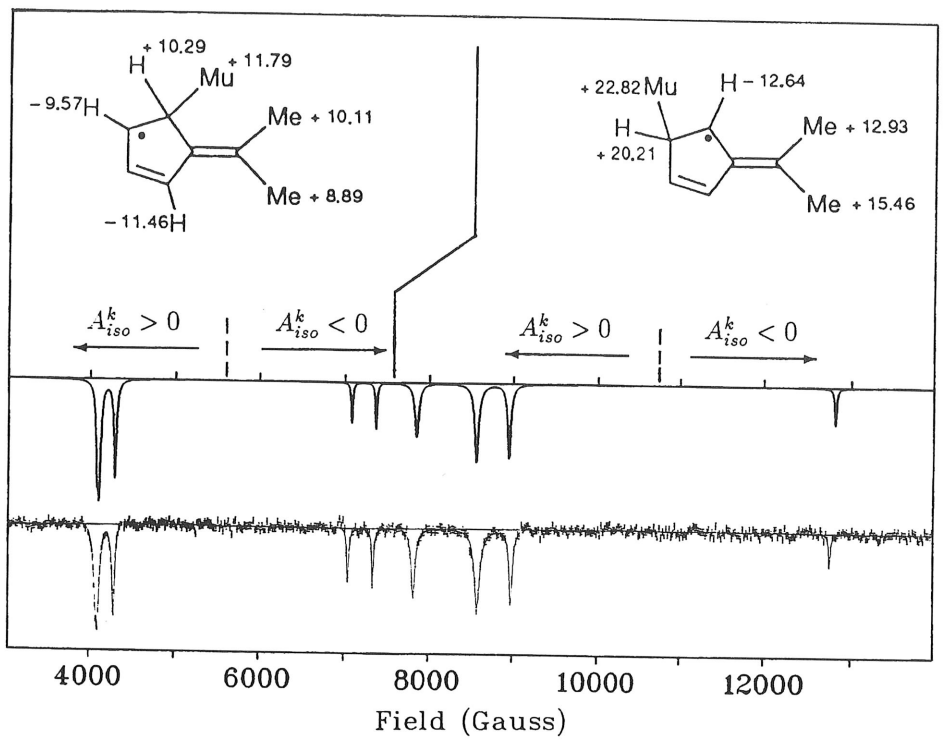

Figure 19. *Experimental ALC–μSR spectrum obtained with 6,6-dimethylfulvene in liquid solution at room temperature (Roduner, 1993). The structures of the two radicals with their coupling constants as derived from the spectrum are given on top.*

is a clear pseudo-static case with narrowing of the lines as temperature increases. The behaviour is understood as a consequence of the spherical shape of C_{60}, in contrast to the ellipsoid shape of C_{70} where rotation about the long axis is clearly preferred, and wobbling of this axis leads to the observed line narrowing. The rotational correlation times extracted for C_{60} are within the range of those determined by other methods (Roduner *et al.* 1995b).

A last example relates to the simulations for cyclohexadienyl radicals shown in Figure 17. Experimental ALC–μSR spectra were obtained with benzene in a silicalite zeolite at a loading of one molecule per unit cell, about one-eighth of the saturation loading. This zeolite is essentially pure quartz with the same structure as HZSM–5, a famous porous catalyst with straight channels intersecting zig-zag channels. These are of slightly elliptical shape and have a mean diameter of about 0.55nm so that benzene molecules fit snugly (Roduner *et al.* 1998). The mobility of reactants, intermediates and products in the pores is of central importance for the proper functioning of the catalyst. Figure 22 displays the experimental spectra which were obtained with this system. The Δ_1 resonance is present, showing the absence of isotropic motion, its shape is that of an axial powder pattern with the steeper slope on the high field side, which demonstrates clearly that there is fast rotation of the radical about an axis perpendicular to the plane of carbon atoms (compare Figure 17). Rotation freezes only below 50 K, as apparent from the

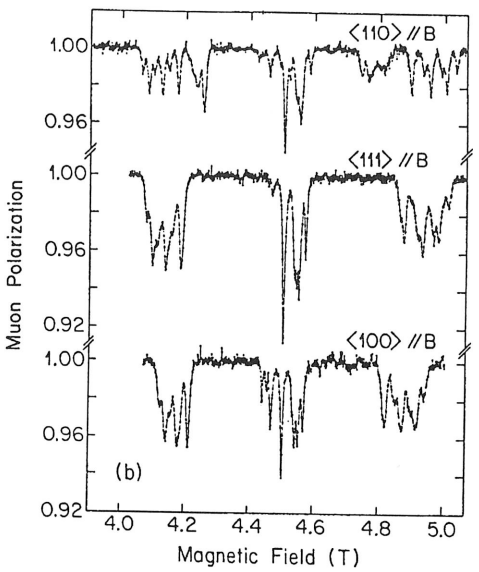

Figure 20. *ALC–μSR spectra obtained with CuCl at T = 100K (from Schneider et al. 1990). The resonances are due to dipolar and quadrupolar couplings of the four nearest Cu and the six next-nearest Cl nuclei to Mu sitting at a tetrahedral interstitial site.*

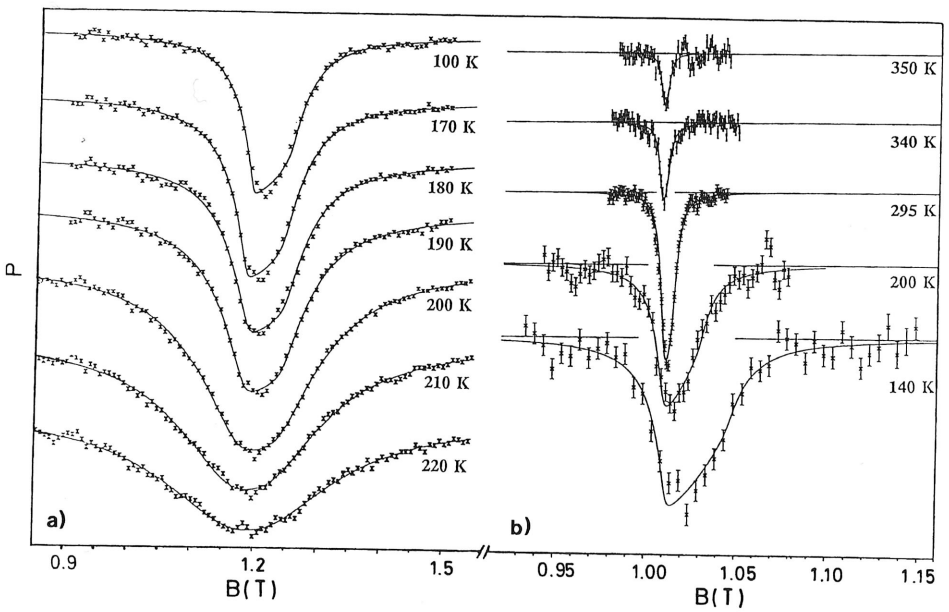

Figure 21. *ALC–μSR spectra obtained upon positive muon irradiation of polycrystalline C_{60} (a) and C_{70} (b). The opposite trends of the line widths with temperature demonstrates two fundamentally different types of dynamics despite the similarity of the two fullerenes (Roduner et al. 1995).*

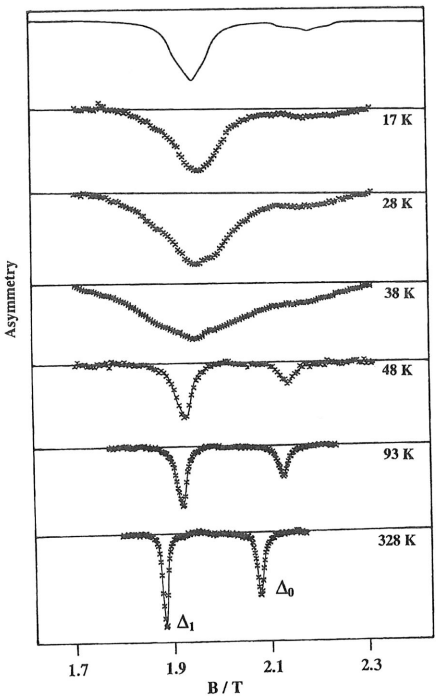

Figure 22. *ALC–μSR spectra observed with benzene in ZSM5 silicalite at different temperatures, giving clear evidence of uniaxial rotation about the axis normal to the molecular plane above 50K (Roduner et al. 1998).*

extreme broadening. At the lowest temperature the system is essentially static on our time scale. The temperature dependence of the hyperfine anisotropy, related to the width of the resonance, is shown in Figure 23, together with the zeolite structure. $D_\perp$ drops dramatically near 100K, demonstrating that there is an aligning potential of the order of 1kJ/mol and a very high and nearly isotropic mobility at room temperature, which seems to be possible only for radicals sitting at the channel intersections. The increase above 450K is attributed to radicals derived from benzene which has diffused into the channels.

Time resolved experiments give the time dependence of muon polarisation directly. Figure 24 shows the oscillations ($aP_z(B,t)$, Equation 10) for measurements on-resonance of a Δ_1 ALC–μSR signal obtained with benzene in ZSM–5 silicalite. This is a powder sample, and according to Equation 7 ν_r depends on orientation. The observed signal is thus a superposition of signals within a range of frequencies, it therefore looks damped. The parameters obtained from fits to these experiments are within error the same as the ones from the time integrated spectra in Figure 9. It should be noted, however, that a time resolved experiment gives direct information about the time dependence which for the derivation about time integral line shapes is only assumed to be known. It is advisable to check this equivalence from time to time.

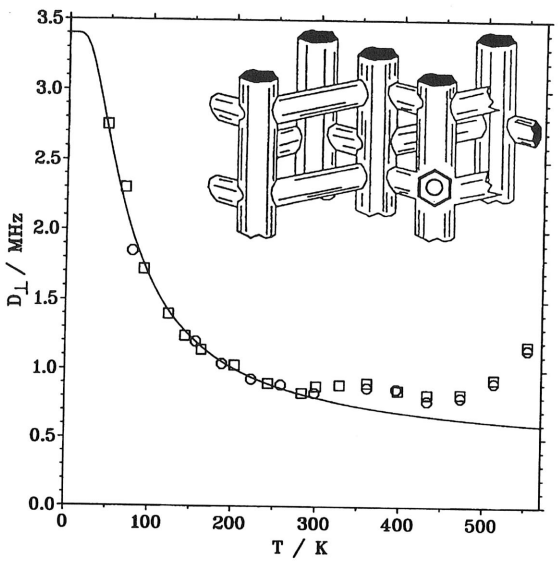

Figure 23. *Muon hyperfine anisotropy and zeolite structure relating to the spectra displayed in Figure 9, demonstrating the high extent of reorientational dynamics of the cyclohexadienyl radical near room temperature.*

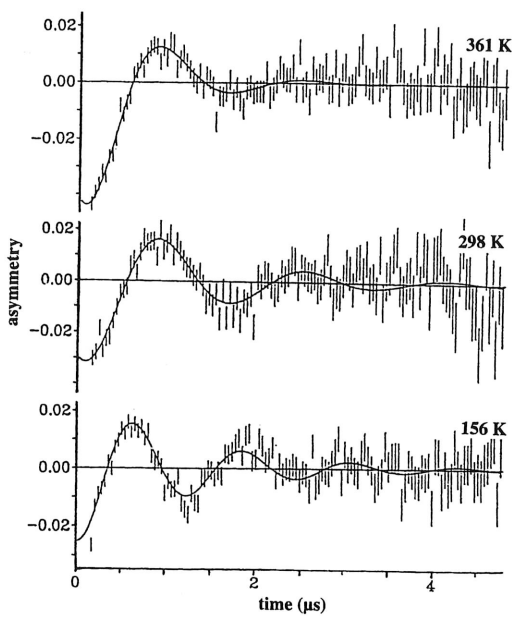

Figure 24. *Time dependent measurements of the muon decay anisotropy obtained with benzene in ZSM–5 silicalite in longitudinal external fields, on-resonance the Δ_1 transition. The oscillations show the time evolution of the non-eigenstate at the avoided crossing.*

3 Spectroscopy of free radicals and other paramagnetic multi-spin systems

3.1 Paramagnetic multi-spin systems

Muons which are stopped in an experimental sample often come to rest in the neighbourhood of nuclei which carry magnetic moments. Since the spatial distribution of these nuclei about the muon may not be well-defined and since the nuclei may relax or the muon diffuse (leading to a time-dependent Hamiltonian), multi-spin interactions of this type are normally treated stochastically, and the experimentally observable quantity is the muon relaxation. This phenomenon is not the subject of the present chapter. Here we shall confine ourselves to the case where there is a limited number of magnetic particles which are characterised by a well- defined time-independent Hamiltonian. Moreover, since direct muon-nuclear interactions are frequently not sufficiently large to lead to features which are spectrally resolved we shall restrict the present treatment to paramagnetic species.

Since the electron magnetic moment is larger than that of the proton by a factor of 1835, and since magnetic interactions are proportional to the magnetic moments of *both* interacting particles, nuclear moments can lead to large contributions to the magnetic energy of a spin system. Mediated by the electron, magnetic nuclei can influence μSR spectra strongly even when the direct muon-nuclear interaction is neglected. This is the subject of the present chapter.

The relevant terms in the Hamiltonian are given in the following scheme (an explicit form is found in the previous section on Avoided-Level-Crossing Spectroscopy):

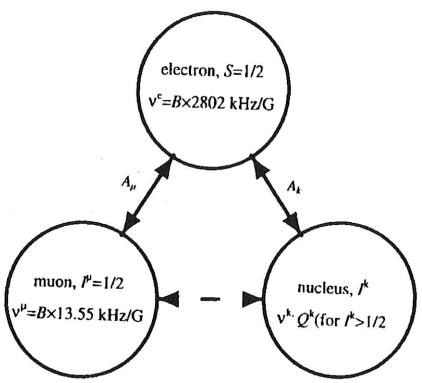

We distinguish three types of particles: (i) the muon with quantum numbers $I^\mu = \frac{1}{2}$ for its spin angular momentum and $m^\mu = \pm\frac{1}{2}$ for its z-component, (ii) n other magnetic nuclei with quantum numbers I^k and $-I^k \leq m^k \leq I^k$, and (iii) the electron characterised by $S = \frac{1}{2}$ and $m^s = \pm\frac{1}{2}$. The muon is treated separately from the other nuclei only because the μSR technique monitors directly the muon transitions. The interaction with the external field B is reflected by the Zeeman precession frequencies ν^μ, ν^k, and ν^e, as given in the scheme. For protons, the Zeeman frequency is $\nu^p = B \times 4.2577$ kHz/G, for all other nuclei it is less. The muon and the nuclei k are coupled to the unpaired electron by the *hyperfine interactions* A_μ, A_k. Certain parts of the literature single out the muon

hyperfine interaction and designate A_k *superhyperfine interaction.*

There are two contributions to the hyperfine interaction: (i) The *Fermi contact interaction* which is isotropic (independent of the orientation of the species in the external field) and is transmitted through chemical bonds or antibonding interactions. (ii) The orientation dependent dipolar part which arises from through-space interaction of magnetic point-dipoles. It scales with $\langle r_{ek}^{-3} \rangle$, where r_{ek} is the electron- nuclear distance. $\langle r_{ek}^{-3} \rangle$ is obtained by integration over the molecular orbital that describes the distribution of the unpaired electron spin, and over the vibrational wave functions which modulate r_{ek}.

A nucleus with $I^k > \frac{1}{2}$ requires an extra term in the Hamiltonian due to its electric nuclear quadrupole moment Q_k which reflects an anisotropic distribution of the nuclear charge. The energy of the interaction depends on the orientation of the nucleus in the local electric field gradient eq due to the distribution of the electron charge in the vicinity of the nucleus. The experimentally accessible parameter is the quadrupole coupling constant, $QCC = e^2qQ/h$.

Here, we are concerned mainly with the effects of additional nuclear spins. To simplify the situation we shall restrict our treatment to isotropic systems. Many aspects of anisotropic systems are recovered when we assume that A_μ and A_k are effective, orientation- dependent properties. In the following we shall also neglect nuclear quadrupole moments.

3.2 Formation and structure of muonated radicals

Muonated free radicals arise formally by addition of Mu to isolated or conjugated double or triple bonds of organic molecules. In many cases Mu is probably also the true physical precursor, but it was shown for example in the case of acetone that the formation process is a mixed one, the second route being consecutive electron-muon addition (Roduner, 1986). In not too high fields, the sense of muon precession and the time scales are different for the two routes of formation, but in order for a radical to be observed in transverse fields the muons should arrive in the radical with coherent phase.

The formation process places the muon two bond lengths away from the radical centre or delocalised system (see Figure 25). Consequently, the unpaired electron density at the muon is much less than in the Mu atom. The isotropic coupling constant A_μ is therefore typically between a few MHz and approximately 700MHz, depending in a well-known way on the structure, and it is of positive sign in almost all cases.

The isotropic hyperfine coupling constants A_p of the protons (or other magnetic nuclei) are related to the radical structure in the same way as A_μ, but in equivalent positions they are reduced by the ratio of magnetic moments, $\mu_p/\mu_\mu = 0.3141$, and on top of this by an intrinsic isotope effect of approximately 20%.

The so-called Mu* state which is observed in semiconductors has the Mu atom in a bond centre site, in silicon for example between two silicon atoms. This Si-Mu-Si species is very similar to an organic free radical. It may be described by two bonds for which three electrons are available, as shown in Figure 26. The original bond between the two silicon atoms A and B is formed by the two sp^3 hybrid orbitals which are the basis for the tetrahedral bond geometry around the atoms. In the ground state, the Mu 1s orbital can overlap constructively with these sp^3 orbitals. The second, non-bonding molecular orbital

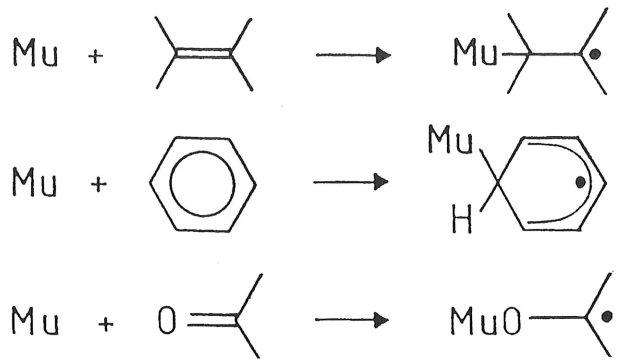

Figure 25. *Muonium addition to tetramethylethene, to benzene, and to the oxygen of acetone. In the adduct to benzene, the cyclohexadienyl radical, the unpaired electron is delocalised over much of π-molecular orbital of the ring.*

contains one nodal plane half way between the two atoms A and B, i.e. exactly through the muon. The third one is highest in energy and arises from antibonding interaction. Two electrons occupy the bonding orbital. The unpaired electron goes into the non-bonding orbital so that to a first approximation the unpaired electron density at the muon is zero. However, its spin polarises the bonding orbital so that a net *negative* spin density is created at the muon. Similar states have been observed in Ge, C (diamond) and in the III-V semiconductors GaAs and GaP (Cox, 1987).

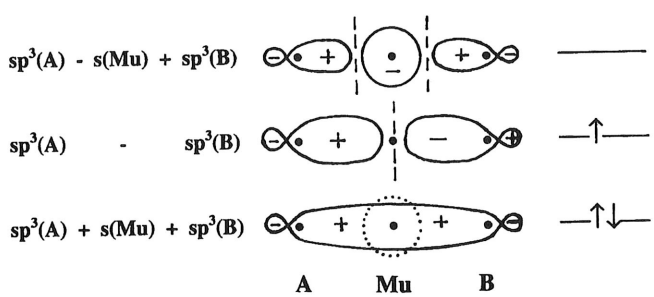

Figure 26. *Molecular orbital diagram describing the bond centre state Mu* in semiconductors.*

Paramagnetic states with properties very close to those of vacuum Mu were observed in alkali halides (Baumeler, 1986). They are best described by interstitial Mu with small couplings to magnetic nuclei of the halide anions or the alkali cations in the first and the second coordination shells. Similar isotropic states are also found in semiconductors, and as far as host atoms carry a nuclear spin the present treatment is applicable to these systems.

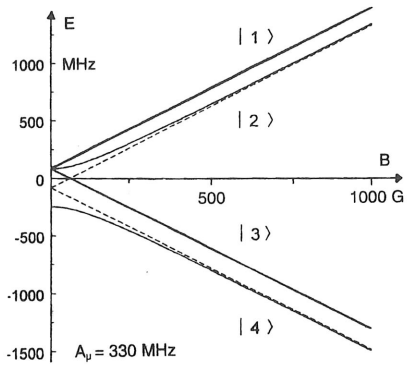

Figure 27. *Breit-Rabi diagram for an muonium-like isotropic muon-electron state with* $A_\mu = 330$ *MHz.*

3.3 Breit-Rabi diagrams

The muonium atom is a muon-electron two-spin-1/2 system. The magnetic energies of the four possible spin states are given by the Breit-Rabi diagram in Figure 27. In the high field limit the eigenstates are pure Zeeman states represented by $|m^s, m^\mu\rangle$:

$$|1\rangle = |\tfrac{1}{2}, \tfrac{1}{2}\rangle, \qquad |2\rangle = |\tfrac{1}{2}, -\tfrac{1}{2}\rangle, \qquad |3\rangle = |-\tfrac{1}{2}, -\tfrac{1}{2}\rangle, \qquad |4\rangle = |-\tfrac{1}{2}, \tfrac{1}{2}\rangle.$$

In the isotropic case, $|1\rangle$ and $|3\rangle$ are pure Zeeman states over the entire field range, but $|2\rangle$ and $|4\rangle$ mix in low fields. In zero field, the two spins combine to a singlet state ($|4\rangle$) and the degenerate triplet states $|1\rangle$, $|2\rangle$, and $|3\rangle$. For anisotropic systems, this degeneracy is lifted into two plus one in axial symmetry and into three individual states in lower symmetry. A full treatment of the isotropic and anisotropic Mu system has been given by Patterson (1988) and by Macrae et al. (1994).

The amplitudes of the transitions between states $|n\rangle$ and $|m\rangle$ are evaluated as the squares of the expectation values for the Pauli spin operators (Roduner and Fischer, 1981):

$$\begin{aligned} &|\langle m|\hat{\sigma}_x|n\rangle|^2 \qquad \text{for transverse fields, and} \\ &|\langle m|\hat{\sigma}_z|n\rangle|^2 \qquad \text{for longitudinal fields.} \end{aligned} \tag{21}$$

In low transverse fields this leads to the four transitions $|1\rangle \leftrightarrow |2\rangle$, $|2\rangle \leftrightarrow |3\rangle$, $|3\rangle \leftrightarrow |4\rangle$, and $|1\rangle \leftrightarrow |4\rangle$, but in high fields only $|1\rangle \leftrightarrow |2\rangle$ and $|3\rangle \leftrightarrow |4\rangle$ are left with significant intensity. In low longitudinal fields only the transition $|2\rangle \leftrightarrow |4\rangle$ is allowed, but its amplitude decreases as the field increases, and in high fields it is forbidden. The only non- zero frequency transition in zero field is $|2\rangle \leftrightarrow |4\rangle$ between the singlet and the triplet state which occurs at the hyperfine frequency A_μ.

We now extend the system by one proton to demonstrate the basic differences between Mu and a multi-spin system. The corresponding Breit-Rabi diagram is shown in Figure 28. The additional spin doubles the number of states, and in zero field they now form three groups, a quartet ($F = \frac{3}{2}$) and two doublet ($F = \frac{1}{2}$) states. Here, F is the quantum number for the total spin angular momentum $\mathbf{F} = \mathbf{S} + \mathbf{I}^\mu + \sum \mathbf{I}^p$, and M_F is the quantum

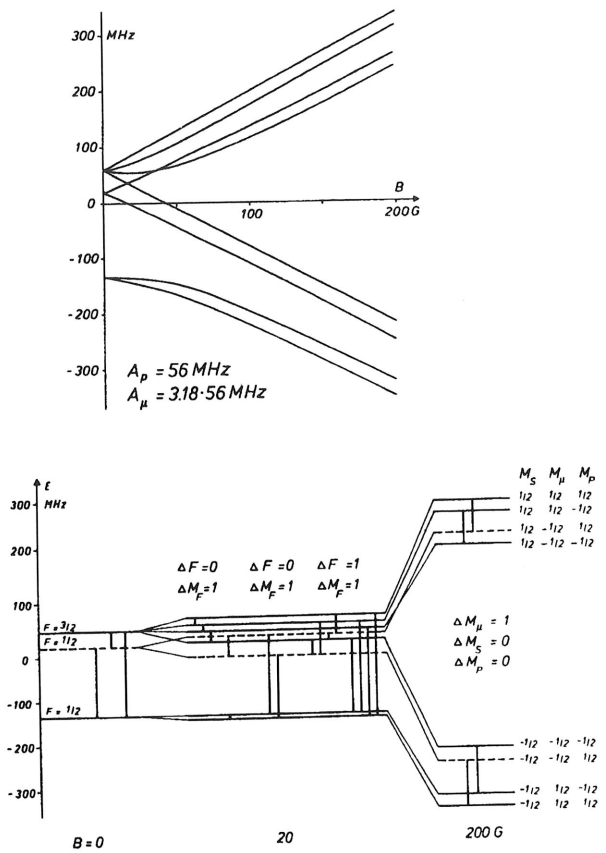

Figure 28. *Breit-Rabi diagram for a muon-electron-proton three-spin-1/2 system with* $A_p = 56$ *MHz and* $A_\mu = 3.18 \times 56$ *MHz* $= 178$*MHz. The zero, intermediate, and high field cases are expanded in the second plot to show the transverse field transitions.*

number for the z-component of $\mathbf{F}$ ($-F \leq M_F \leq F$). The nomenclature $|F, M_F\rangle$ is exact only in zero field but it is often used also in low fields. In high fields, we classify according to the Zeeman states, $|m^s, m^\mu, m^p\rangle$.

The selection rules are obtained from the Fermi golden rule (Equation 1). They are

$$\Delta F = 0, \pm 1 \ ; \qquad \text{in zero and low fields} \tag{22}$$

and in addition

$$\begin{aligned} \Delta M_F &= 0 \qquad \text{in low longitudinal fields, and} \\ \Delta M_F &= \pm 1 \qquad \text{in low transverse fields.} \end{aligned} \tag{23}$$

For high transverse fields one obtains

$$\Delta m^\mu = \pm 1, \ \ \Delta m^s = 0, \ \ \Delta m^p = 0. \tag{24}$$

As for Mu, there are no allowed transitions in high longitudinal fields.

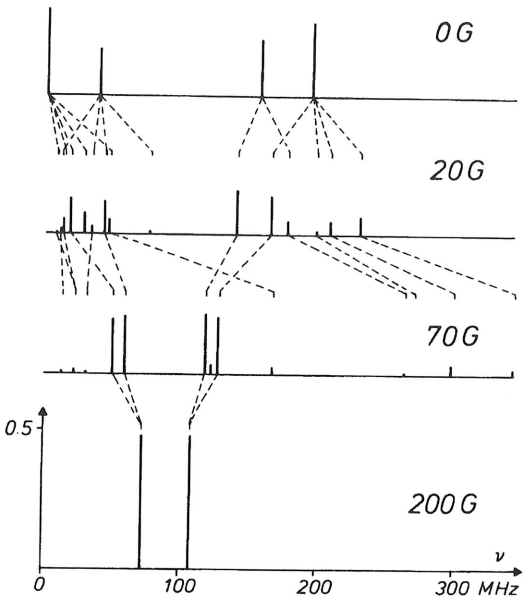

Figure 29. *Calculated muon spin rotation spectrum in zero, intermediate and high field for the muon-electron-proton system of Figure 4.*

All three possible transitions are allowed in zero field, and it is obvious that the highest frequency is the sum of the other two.

15 transitions are allowed in intermediate cases where the external field is of the order of the hyperfine field (here 56MHz / 2.8025MHzG^{-1} = 20 G). The number of transitions increases rapidly with additional spins (Roduner and Fischer, 1981). The muon polarisation is then distributed over very many lines so that it requires extremely high counting statistics in experiments to obtain amplitudes which exceed the noise level.

Four transitions with non-negligible amplitude remain in a transverse field of 200G which is high compared with the hyperfine field. Under these conditions, the proton is decoupled from the muon to a good approximation, so that the four transitions appear in pairs of two degenerate lines, independent of the magnitude of A_p.

Figure 29 displays the muon spin resonance spectra corresponding to the system in zero and in three different transverse fields. The broken lines indicate the dependence of the frequencies on the external field. It is obvious that at fields on the order of the hyperfine field (here 20G) the situation is the most complicated, but it simplifies rapidly as the field increases. The two-line spectrum at 200G is represented by the ENDOR (Electron Nuclear Double Resonance) condition, which is in first order

$$\nu_{\pm} = \left| \nu^{\mu} \pm \frac{1}{2} A_{\mu} \right| . \tag{25}$$

At 200G, ν^{μ} amounts to 2.71MHz, and $\frac{1}{2}A_{\mu}$ to 89MHz. Thus, ν_{-} is negative, but a Fourier transform of a simple experiment does not reveal the sign of the muon precession, so that the line appears reflected at zero in the region of positive frequencies. While in not too

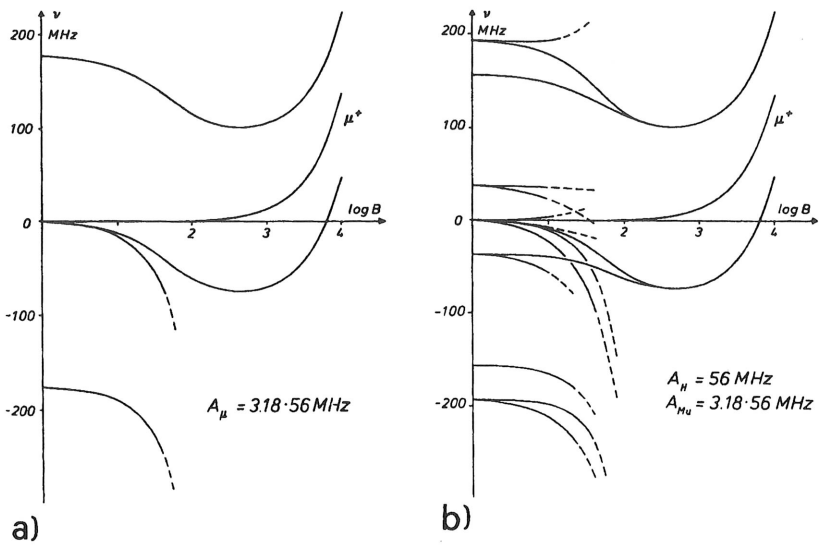

Figure 30. *Dependence of transverse field μSR frequencies on the external field on a log scale. Broken lines indicate low amplitudes. a) $\mu - e$ system, b) $\mu - e - p$ system.*

high fields Equation 5 gives the position of the individual lines only approximately, the sum of the two is *exactly* A_μ.

The important conclusion is that the spectra simplify enormously in high fields, and independent of the number of coupling nuclei we obtain two lines from which the muon hyperfine coupling is calculated. The drawback of this simplification is that any information about other nuclei is lost.

An alternative representation of the field dependence of the frequencies in Mu and in a $\mu - e - p$ system is displayed in Figure 30, which also gives the sign of muon precession relative to that of μ^+. The situation is symmetric in zero field. The superposition of the two equal frequencies with opposite sign reflects the absence of a defined precession axis. Experimentally observable is only a forward-backward *oscillation*, and a counter placed in a direction perpendicular to that of the initial muon polarisation should not show a signal.

In low fields, the two low frequency *muonium precessions* are degenerate and of negative sign (Figure 30a). With increasing field, two of the frequencies gain intensity at the cost of the others which die out. At a field corresponding to $A_\mu \times 36.72$ Gauss (for A_μ in MHz) the negative frequency crosses zero (this is the field where a Δ_1 resonance may appear in ALC–μSR spectroscopy), and the two high field frequencies are displaced symmetrically about ν^μ as required by the ENDOR condition.

The high field side of Figure 30b, showing the three spin system, looks the same as for the Mu analogous two spin system in Figure 30a, because the proton is decoupled. In zero field we have of course again a symmetric situation, but there are more frequencies, and at intermediate fields we have the many low amplitude frequencies.

Additional coupled nuclei will not change the high field behaviour. The zero field

and in particular the intermediate field situation will become very complex, however. We learn that in presence of coupled nuclear moments we should work in high fields, and possibly in moderately high fields where the line splitting gives limited information about nuclear couplings. Only in exceptional cases it is expected that zero or intermediate field experiments reveal detailed information.

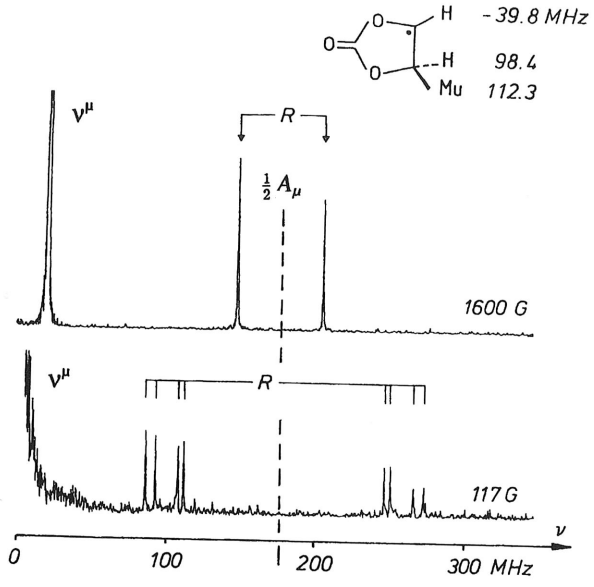

Figure 31. *Fourier spectrum obtained from time differential transverse field μSR with liquid vinylene carbonate at 300K in a transverse field of 1600G (top) and 117G (bottom). The lines R arise from the radical formed by Mu addition to the vinylene double bond. They are displaced symmetrically from $A_\mu/2$ (adapted from Roduner, 1993).*

3.4 Examples of μSR spectra of multi-spin systems

3.4.1 Vinylene carbonate

An instructive example for the theoretically derived principles was obtained with vinylene carbonate, an organic molecule with only two protons at a double bond to which Mu can add. The radical structure is sketched in Figure 31, and the spectra measured in high, intermediate and low transverse fields are given in Figures 31 and 32. A strong line at the Zeeman frequency ν^μ shows that a certain fraction of muons arrives in a diamagnetic environment, but this is not of interest in the present context. In a high external field of 1600G there are two radical lines centred at $\frac{1}{2}A_\mu = 178.7$ MHz and displaced by approximately $\pm\nu^\mu$. The muon hyperfine coupling constant, $A_\mu = 357.5$ MHz is obtained directly from the sum of the two frequencies. Its reduced value, $A'_\mu = A_\mu \times \mu_p/\mu_\mu = A_\mu \times 0.3141 = 112.3$ MHz, is given in Figure 31 for comparison with $A_p = 98.4$ MHz of the proton which is bound to the same carbon. This reveals a hyperfine isotope effect of a

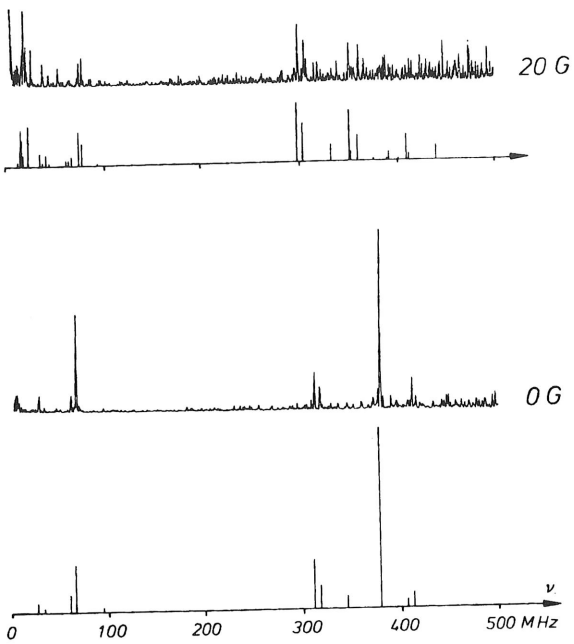

Figure 32. *Observed and simulated μSR spectra of the Mu adduct to vinylene carbonate in low transverse and zero magnetic field. The apparent increase of noise level at high frequencies is a consequence of deconvolution for instrumental time resolution (adapted from Roduner, 1993).*

factor of 1.14 by which A_μ is larger than A_p. It is due to the bond which in the vibrational average is longer for C-Mu than for C-H. The proton coupling constants, including their signs relative to that of the muon, are derived from the 117G spectrum by iterative numerical diagonalisation of the energy matrix until the transitions matched the observed frequencies. Sign and magnitude of the couplings are compatible with expectation.

The most general case of a spectrum is obtained in a field of 20G where the entire muon polarisation is distributed over 56 transitions (Figure 32, top). This leaves very little intensity for individual lines, but comparison of the experimental spectrum with a simulation based on the 117G spectrum gives quite satisfactory agreement of the more intense features. A more favourable situation is attained in zero field, where the number of transitions reduces to 12 only.

The option of zero field spectra is particularly attractive for powders: the hyperfine anisotropy which in presence of external fields broadens the lines does not play a role in zero field so that single crystal like spectra are obtained.

3.4.2 Toluene

Splitting of radical lines in not too high fields may be used for the assignment of radical lines to structures, providing that different protons have greatly different hyperfine inter-

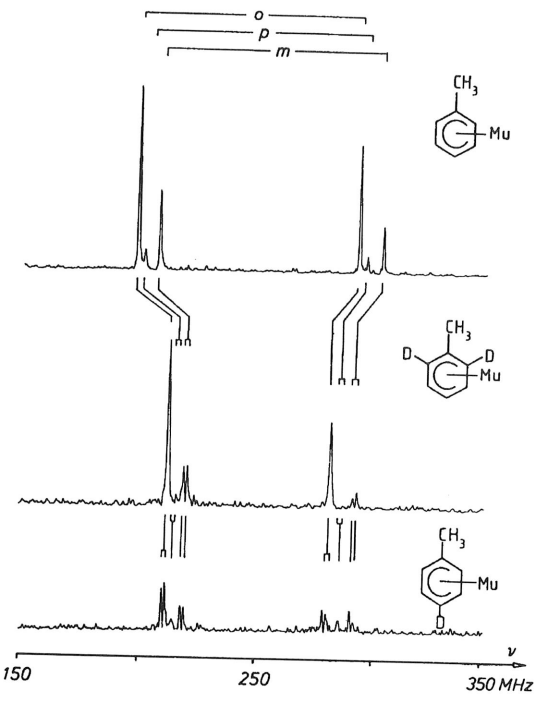

Figure 33. *Radical frequencies of the Mu adducts to toluene in the ortho (o), meta (m), and para (p) positions to the methyl substituent. The assignment rests on the line splitting behaviour in selectively deuterated toluene (Roduner, 1988).*

actions. Use of this has been made in benzene derivatives. In benzene itself all six carbon atoms are equivalent, and only one Mu adduct with $A_\mu = 514.6$ MHz is observed. The protons in this cyclohexadienyl radical have couplings of 126.2MHz (methylene position, the same carbon where the muon is attached), 25.2MHz (for the two ortho protons, next to the position of Mu addition), 7.5MHz (for the two meta protons), and 36.3MHz (for the para proton, across the ring from the position of Mu addition). It can be shown that in a field of 3000G the two radical lines are unsplit, but at 1000G each of them splits into a doublet by about 1.2MHz. If the protons are replaced by deuterons which have a smaller magnetic moment by a factor of 6.5, then the lines are not split in a field of 1000G (Roduner, 1988) (Figure 33).

The case with toluene (methyl benzene) reveals three inequivalent radicals with muon hyperfine couplings of 489.6MHz, 496.3MHz, and 509.3MHz, and the question is the identification of the structures. Here, deuteration of the ortho and para positions helps: the 489.6MHz lines are unsplit in a field of 1000G for the ortho-dideutero-toluene, identifying the radical as the ortho adduct; for the para-deutero-toluene the 496.3MHz line is unsplit, identifying the radical as the para adduct so that the 509.3MHz species must be the meta adduct (Roduner and Fischer, 1981).

A related splitting behaviour in not too high fields allowed the identification of anomalous muonium in GaAs as a bond-centre species as reported by Kiefl et al. (1987).

References

Abragam A, 1984, *C R Acad Sci, Paris* **299** 95.

Baumeler H *et al.* 1986, Hyperfine Interact **32** 659.

Claxton T A and Graham A M, 1987, J Chem Soc Faraday Trans 2, **83** 2307.

Cox S F J, 1987, *J Phys C: Solid State Phys* **20** 3187.

Dilger H *et al.* 1996, *J Phys Chem* **100** 6561 and 16445.

Eck T G, Foldy L L, and Wieder H, 1963, *Physical Review Letters* **10** 239.

Eckart C, 1930, Phys Rev **35** 1303.

Kiefl R F *et al.* 1987 *Phys Rev Letters* **58** 1780.

Garrett B C and Schenter G K, 1994, *Structure, Energetics and Reactivity in Aqueous Solution* ed C J Cramer and D G Truhlar, ACS Symposium Series 568, American Chemical Society, Washington DC.

Glasstone S, Laidler K J, Eyring H, 1941, *The Theory of Rate Processes*, (McGraw-Hill, New York).

Heming M *et al.* 1986, *Chemical Physics Letters* **128** 100.

Kramers H A, 1940, *Physica* (Utrecht) **7** 284.

Kreitzman S R, Roduner E, 1995, *Chem Phys* **192** 189.

Lossack A and Roduner E, unpublished results.

Macrae R M *et al.* 1994, *J Phys Chem* **98** 12133.

Patterson B C, 1988, *Rev Modern Phys* **60** 69.

Roduner E, 1986, *Radiat Phys Chem* **28** 75.

Roduner E, 1988, *The Positive Muon as a Probe in Free Radical Chemistry* (Lecture Notes in Chemistry **49,** Springer, Heidelberg, 1988).

Roduner E, 1990, *Hyperfine Int* **65** 857.

Roduner E, 1993, *Chem Soc Rev* **22** 337.

Roduner E and Fischer H, 1981, *Chem Phys* **54** 261.

Roduner E and Münger K, 1984, *Hyperfine Interact* **17-19** 793.

Roduner E and Reid I D, 1989, *Israel J Chem* **29** 3.

Roduner E *et al.* 1990, *Ber Bunsenges Phys Chem,* **94** 1224.

Roduner E and Bartels D M, 1992, *Ber Bunsenges Phys Chem* **96** 1037.

Roduner E *et al.* 1995, *J Chem Phys* **102** 5989.

Roduner E *et al.* 1995a, *J Chem Soc Faraday Trans* **91** 1935.

Roduner E *et al.* 1995b, *Chem Phys* **192** 231.

Roduner E *et al.* 1998, *J Phys Chem* **102** 7591.

Spaeth J-M, 1986, *Hyperfine Interact* **32** 641.

Schneider J W *et al.* 1990, *Hyperfine Int* **64** 543.

Tregenna-Piggott P L W, Roduner E, Santos S, 1995 *Chem Phys* **203** 317.